

Supporting Information

Water bridges anchored by a C-H \cdots O Hydrogen Bond - The Role of Weak Interactions in Molecular Solvation

Aditi Bhattacharjee[#] and Sanjay Wategaonkar^{*}

Department of Chemical Sciences, Tata Institute of Fundamental Research, Homi Bhabha Road, Mumbai 400 005, India

[#] Present address: Department of Chemistry, University of California, Berkeley, California 94720, USA

Experimental Details

BIM and MBIM were purchased from Sigma-Aldrich and used without further purification. The sample vapours were seeded in He and expanded into a vacuum chamber through a pulsed nozzle. The water clusters were prepared by using a premix of H₂O vapor in helium (~0.5%) as the backing gas. An Nd³⁺:YAG pumped (Quantel YG781C, 10Hz, FWHM ~6ns) dye laser (Quantel TDL70) was used as the excitation laser while another Nd³⁺:YAG pumped (Quantel Brilliant, 10 Hz, FWHM ~5ns) dye laser (Pulsare, Fine Adjustment) was used as the ionization laser. The ionization laser was set at a fixed wavelength below the ionization threshold of the species. The excitation laser was independently calibrated by recording etalon fringe spectrum as well as by the optogalvanic method. For the IR measurements, a LiNbO₃ optical parametric oscillator (OPO) (LaserSpec, Belgium) was used with an intracavity etalon (~0.5 cm⁻¹). KTP OPO was used to cover the spectral region where the LiNbO₃ absorbs (~3480-3510 cm⁻¹). Photoacoustic IR spectra of water vapor, NH₃ and CH₄ gas were recorded in the regions of 4000-3500 cm⁻¹, 3500-3200 cm⁻¹ and 3150-2900 cm⁻¹, respectively, and compared with the reference lines provided in the HITRAN database for calibration of the IR OPO.^[1] The IR spectra were measured separately in the O-H, N-H and C-H regions (by monitoring the fluorescence signal at the resonance position of the individual features, i.e. using fluorescence depletion by infrared spectroscopy, also called FDIR spectroscopy) and later combined together in one plot. Since C-H has much weaker oscillator strength than O-H and N-H, higher IR power was used in the C-H region (except in the case where a red-shifted H-bonded O-H appeared in the C-H region to avoid saturation of the dip). Typical IR pulse energies used in the experiment were ~ 1 mJ in the O-H and N-H regions and ~3 mJ in the C-H region. All three lasers were spatially overlapped and temporally synchronized so that the excitation and ionization pulses arrived at the same time whereas the IR pulse preceded the excitation pulse by ~ 50 ns.

Computational methods

Quantum chemical calculations were carried out using the Gaussian 09 suite of programs.^[2] A variety of chemically intuitive initial geometries were optimized for each water cluster with both DFT (B3LYP as well as dispersion corrected functionals like M06-2X, LC- ω PBE and ω B97X-D) and MP2 methods using 6-311++G** and aug-cc-pVDZ basis sets. They were subsequently subjected to harmonic frequency calculations for comparison with the experiment. The binding energies of the complexes were corrected for the zero point energy (ZPE) and basis set superposition error (BSSE). In addition, the geometries of the global minimum structures predicted at all levels of calculation which also matched our spectroscopic data best were further refined by optimization on counterpoise-corrected (cp) surface at the B3LYP and MP2 levels to obtain more accurate frequencies and binding energies. We support our experimental data with computational results obtained mainly at the cp-B3LYP and cp-MP2 levels of theory using the aug-cc-pVDZ basis set. As geometry optimization on counterpoise-corrected surface is computationally expensive, it was not carried out for other structures corresponding to local minima which were not observed experimentally.

FIGURES

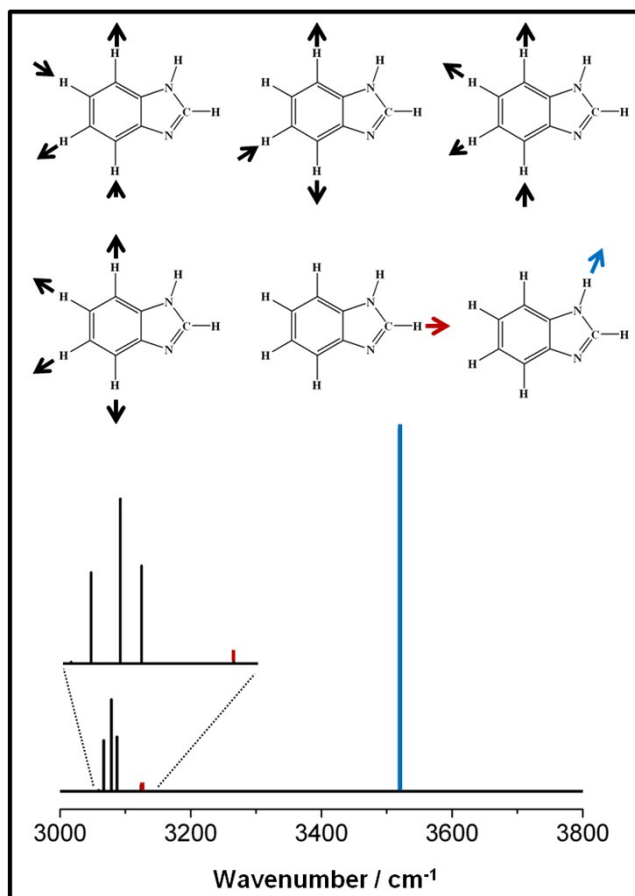
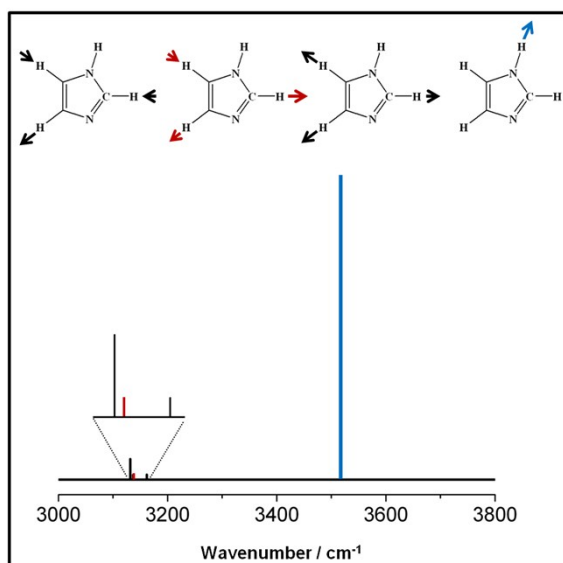


Figure S1: The normal modes of imidazole (top) and BIM (bottom) and their computed vibrational spectra at the B3LYP/aug-cc-pVDZ level of theory. The blue line indicates the position of the N-H stretching frequency. The C-H stretching vibrations are coupled in imidazole; the red line depicts the mode with the highest amplitude on the C(2)-H. This coupling is removed in BIM, where the stretching vibration of the C(2)-H (shown in red) in the imidazole ring is rendered a local oscillator.

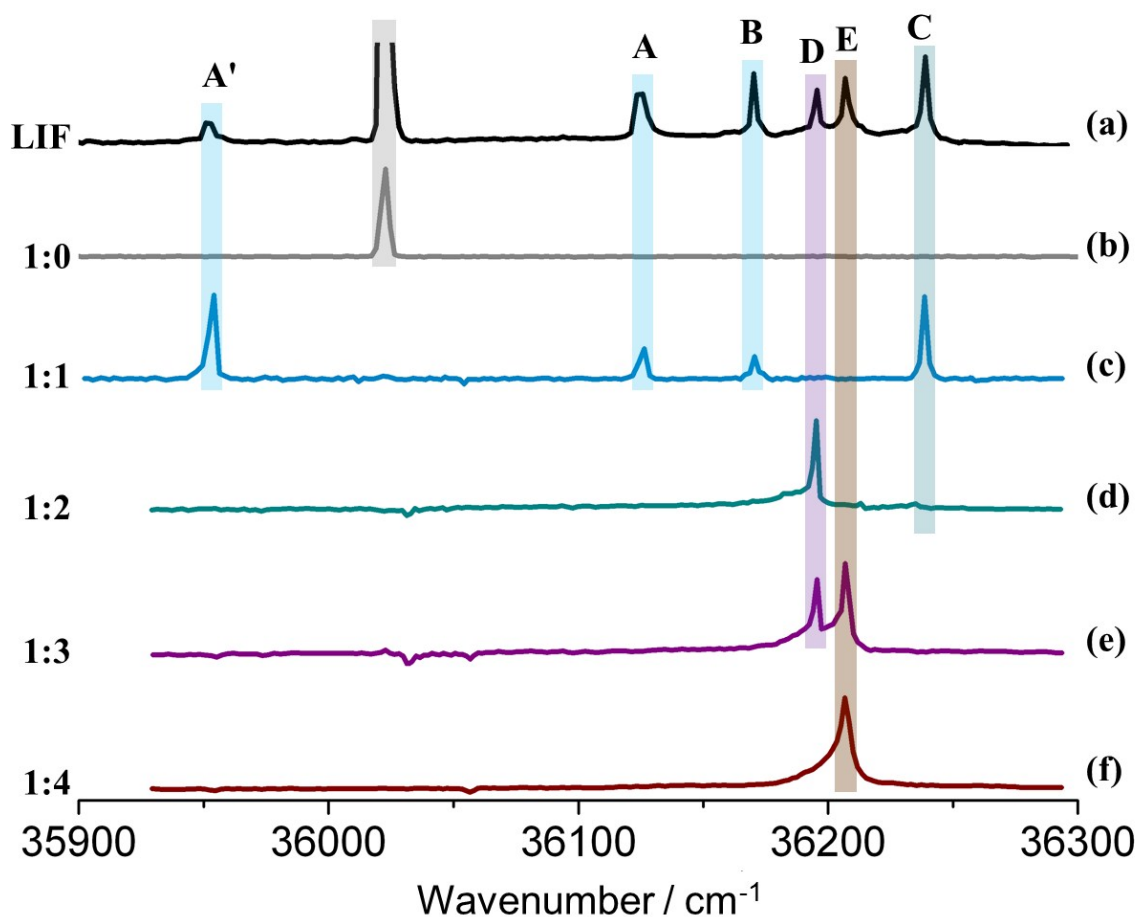


Figure S2: (a) LIF spectrum of BIM in presence of water (zoomed to show the W_n features clearly). (b-f) 2cR2PI spectra of BIM- W_n clusters ($n=0-4$) obtained by fixing the ionization laser at ~ 32785 cm^{-1} while scanning the pump laser. Vertical bars are provided to illustrate the assignment of the features obtained in the LIF spectrum. The water clusters were found to undergo extensive fragmentation upon photoionization and every W_n cluster dissociated into the $W_{(n-1)}$ mass channel (traces c-f). Similar fragmentation has also been reported for the hydrated clusters of 4-phenylimidazole.^[3] The BIM- W_2 complex was found to be unstable in the excited state and completely dissociated to give the peak at 36239 cm^{-1} in the BIM- W_1 mass channel (c). Conclusive proof for this assignment comes from the measured IR spectra.

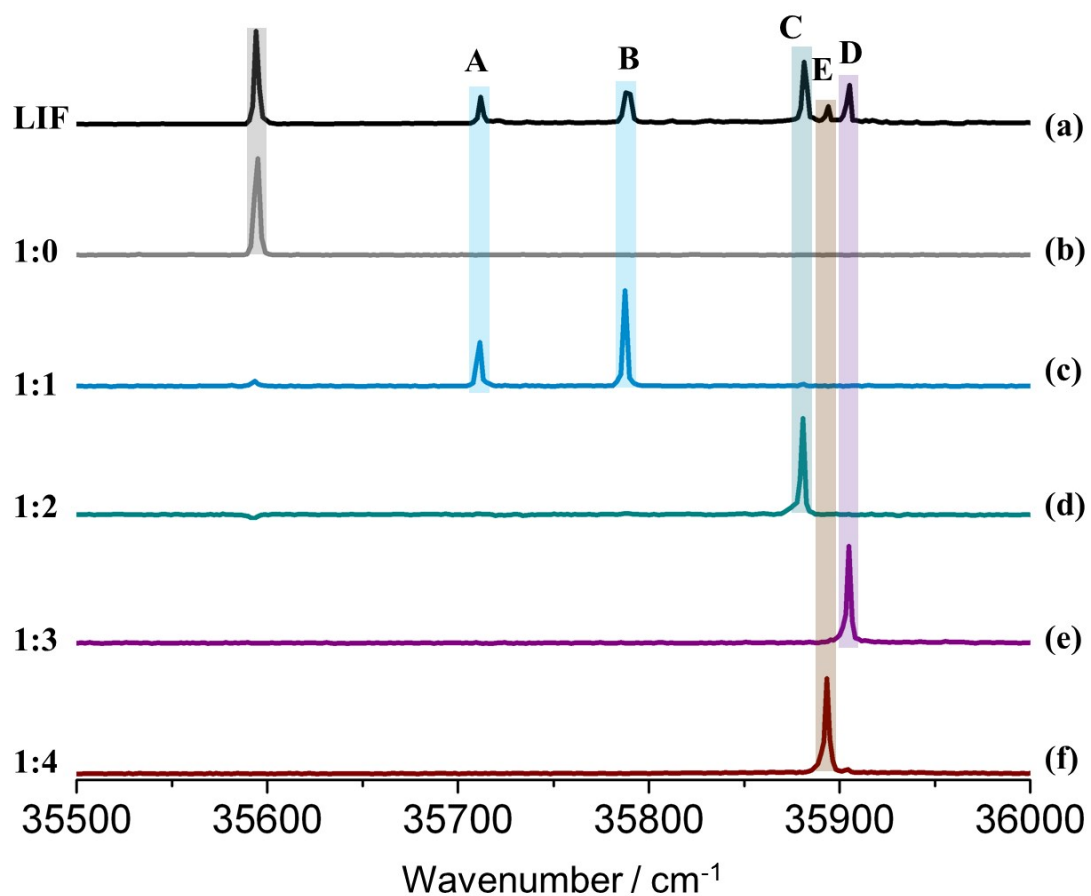


Figure S3: (a) LIF spectrum of MBIM in presence of water. (b-f): 2c-R2PI spectra of MBIM- W_n clusters ($n=0-4$). The ionization laser was fixed at ~ 32260 cm^{-1} . Vertical bars are provided to illustrate the assignment of the features obtained in the LIF spectrum. The water clusters of MBIM were stable upon excitation and subsequent ionization, i.e. no fragmentation was observed in this case.

Figures S4.1 to S4.3 and S5.1 to S5.3 provide a detailed comparison of the free OH (S4.1, S5.1), NH and bound OH(S4.2, S5.2), and the CH (S4.3, S5.3) regions of the FDIR spectra of BIM- W_n and MBIM- W_n with the computed stick spectra obtained at the cp-B3LYP/aug-cc-pVDZ and MP2/aug-cc-pVDZ levels of theory.

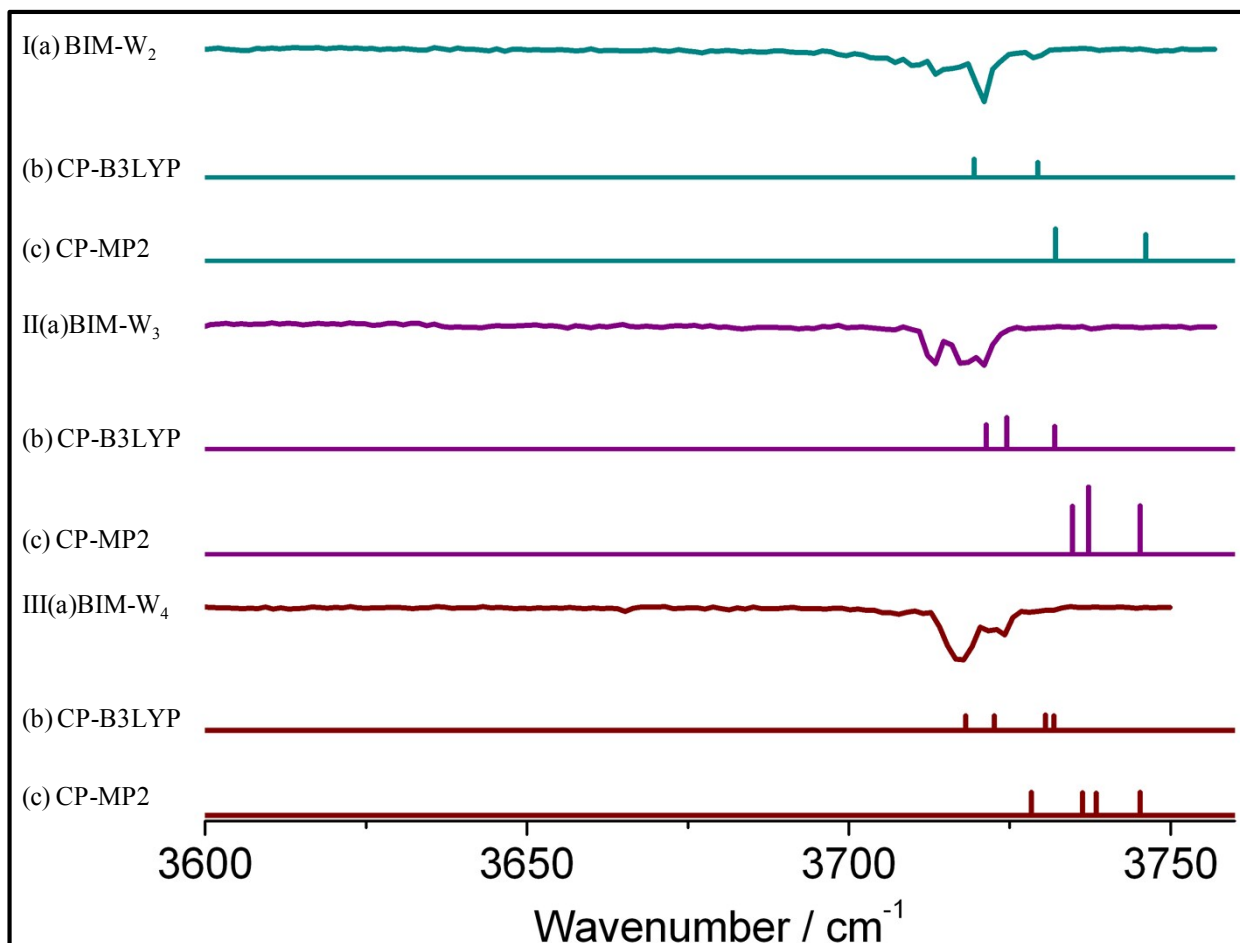


Figure S4.1: Observed FDIR spectra (Ia, IIa, IIIa) of BIM- W_n ($n=2-4$) in the free OH stretching region compared with the stick spectra computed at the cp-B3LYP/aug-cc-pVDZ (scaled by 0.9634) (Ib, IIb, IIIb) and cp-MP2/aug-cc-pVDZ levels (scaled by 0.9620) (Ic, IIc, IIIc). Typical full-width at half-maximum (FWHM) for free-OH peak is $\sim 2.5 \text{ cm}^{-1}$. The broad dip at 3718 cm^{-1} in III(a) has FWHM of 4 cm^{-1} and consists two overlapping transitions which could not be resolved even in high resolution (0.4 cm^{-1}) scans.

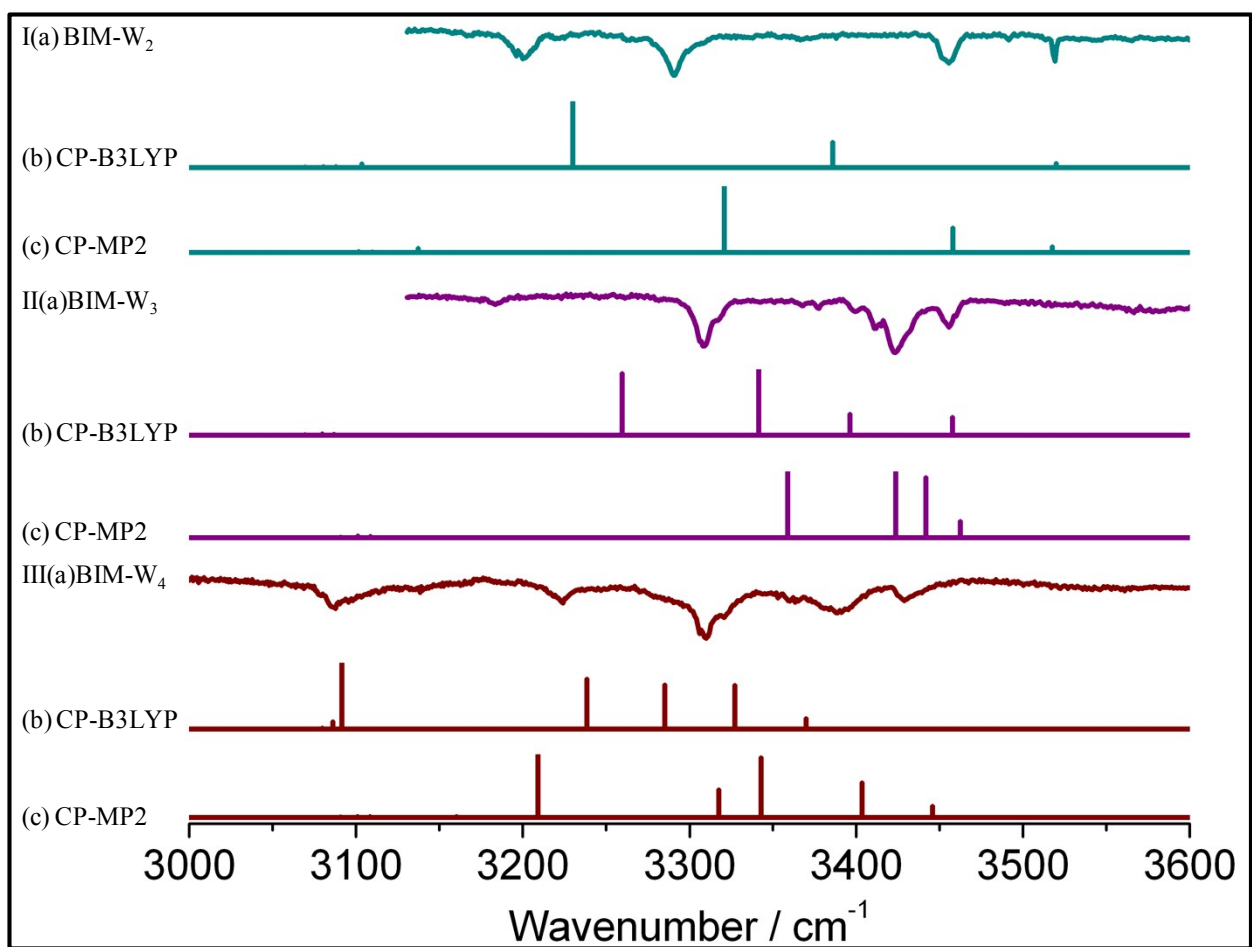


Figure S4.2: Observed FDIR spectra (Ia, IIa, IIIa) of BIM- W_n ($n=2-4$) in the NH and hydrogen bonded OH stretching region compared with the stick spectra computed at the cp-B3LYP/ aug-cc-pVDZ (scaled by 0.9634) (Ib, IIb, IIIb) and cp-MP2/ aug-cc-pVDZ levels (scaled by 0.9620) (Ic, IIc, IIIc).

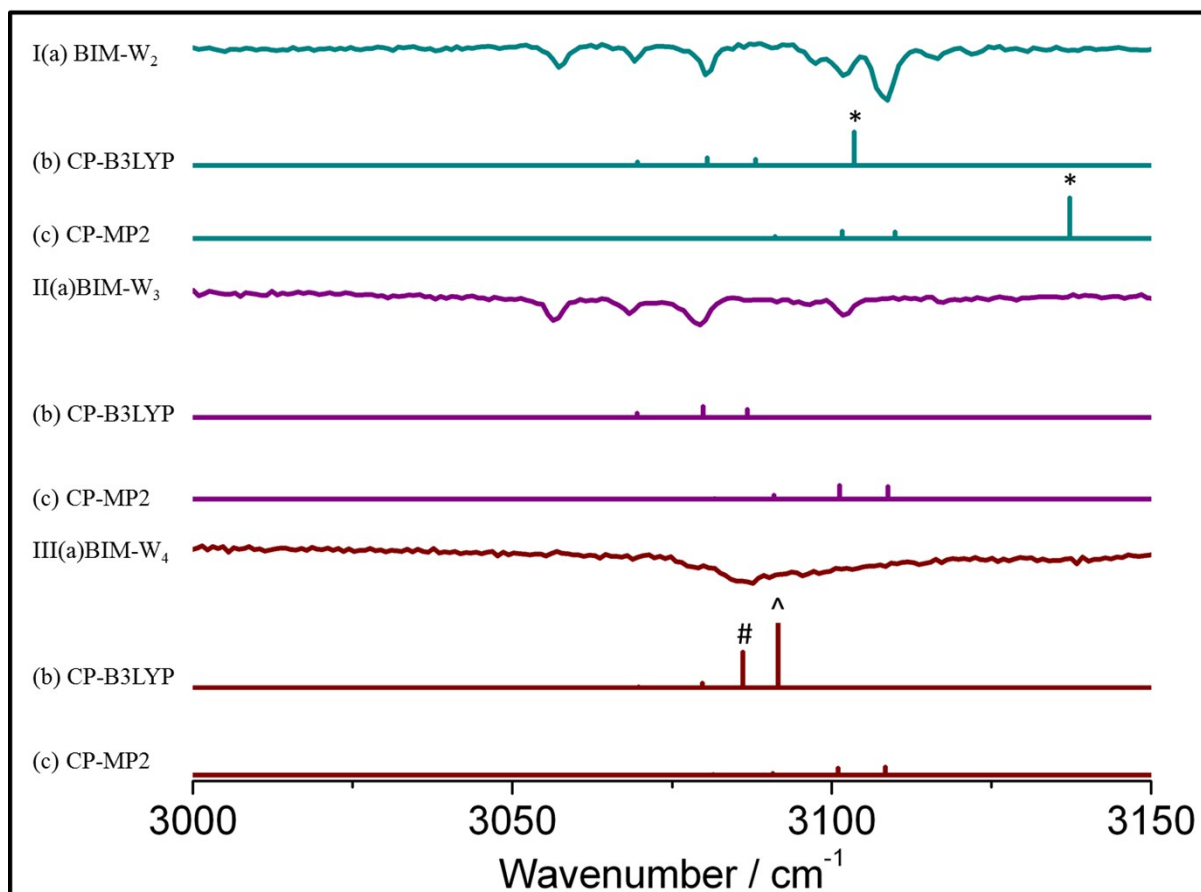


Figure S4.3: Observed FDIR spectra (Ia, IIa, IIIa) of BIM-W_n (n=2-4) in the CH stretching region compared with the stick spectra computed at the cp-B3LYP/ aug-cc-pVDZ (scaled by 0.9634) (Ib, IIb, IIIb) and cp-MP2/ aug-cc-pVDZ (scaled by 0.9620) (Ic, IIc, IIIc) levels. Peak marked * indicate an enhanced C(2)-H while the one marked ^ represents a bonded O-H stretch. The enhanced C-H (marked #) to the left of the bound O-H (marked ^) in III(b) is not the C(2)-H but the symmetric vibration of the C-H bonds in the phenyl ring which is found to be mixed with the bound OH at the cp-B3LYP/aug-cc-pVDZ level (such mixing and consequent enhancement was found to be absent at the MP2 level).

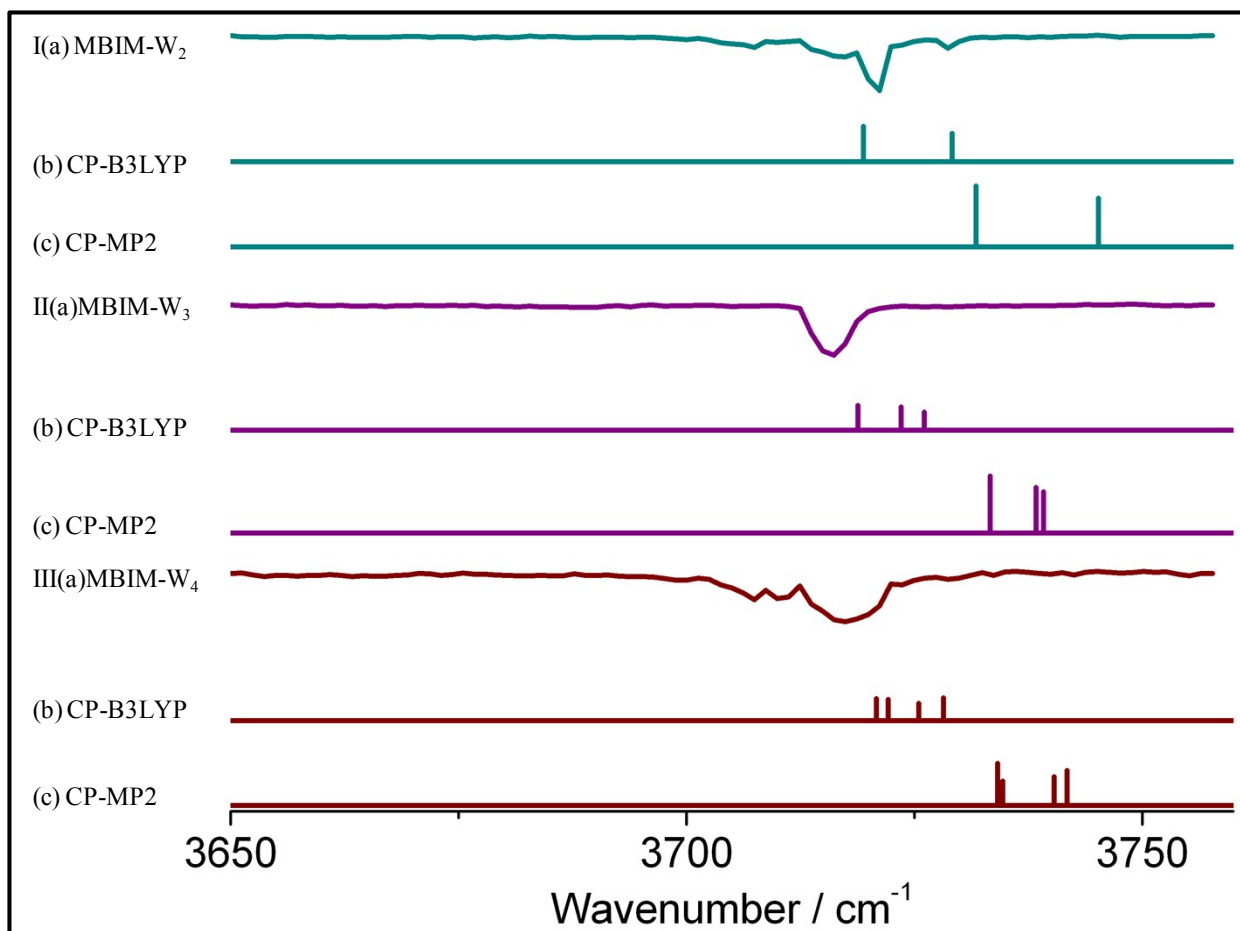


Figure S5.1: Observed FDIR spectra (Ia, IIa, IIIa) of MBIM- W_n ($n=2-4$) in the free OH stretching region compared with the stick spectra computed at the cp-B3LYP/ aug-cc-pVDZ (scaled by 0.9634) (Ib, IIb, IIIb) and cp-MP2/ aug-cc-pVDZ (scaled by 0.9620) (Ic, IIc, IIIc) levels. Typical full-width at half-maximum (FWHM) for free-OH peak is ~ 2.5 cm^{-1} . The broad dip at 3716 cm^{-1} in II(a) has FWHM of 4.5 cm^{-1} and has three overlapping transitions which could not be resolved even at high (0.4 cm^{-1}) resolution. Similarly, the broad dip at 3717 cm^{-1} in III(a) has a FWHM of 7.4 cm^{-1} and constitutes two overlapping transitions that could not be resolved.

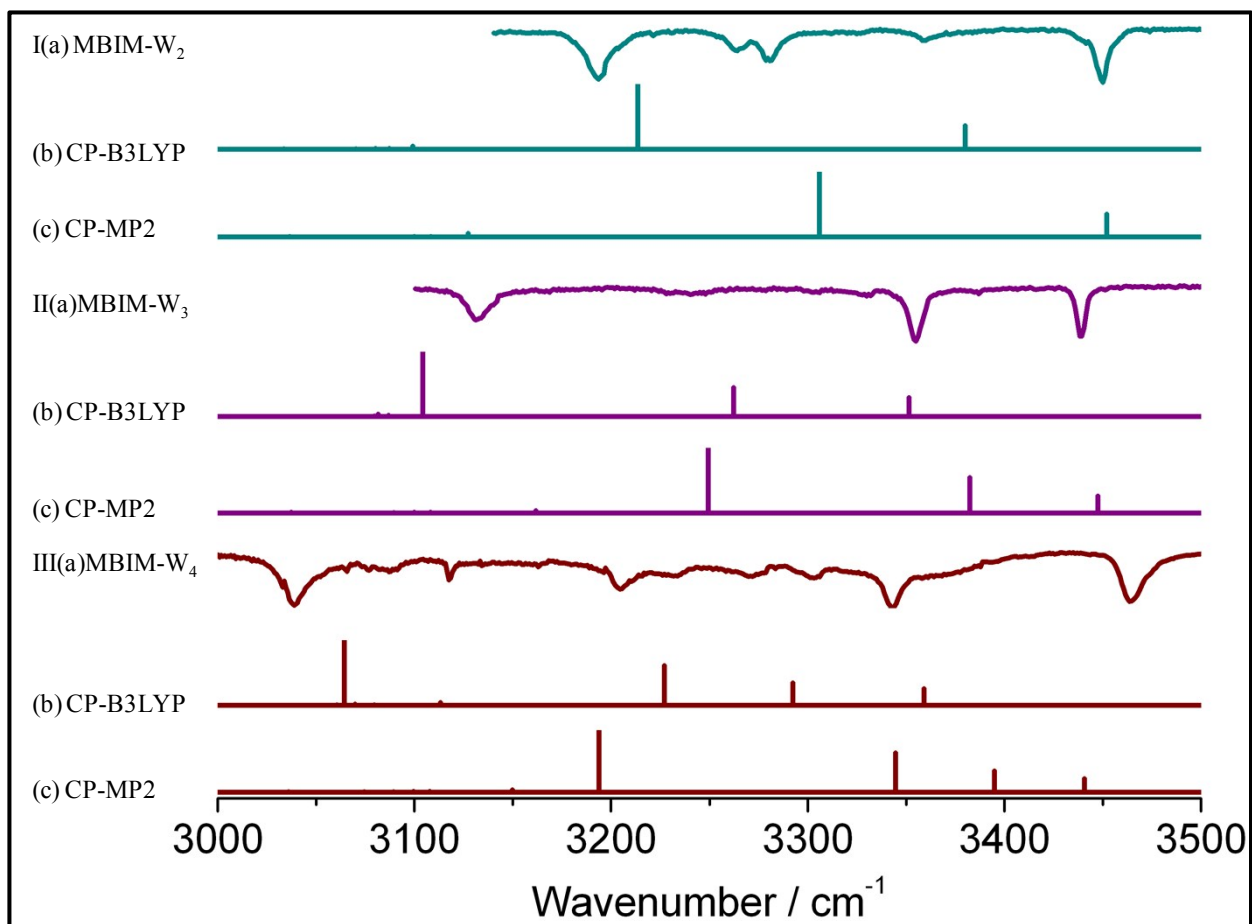


Figure S5.2: Observed FDIR spectra (Ia, IIa, IIIa) of MBIM- W_n ($n=2-4$) in the hydrogen bonded OH stretching region compared with the stick spectra computed at the cp-B3LYP/aug-cc-pVDZ (scaled by 0.9634) (Ib, IIb, IIIb) and cp-MP2/ aug-cc-pVDZ levels (scaled by 0.9620) (Ic, IIc, IIIc).

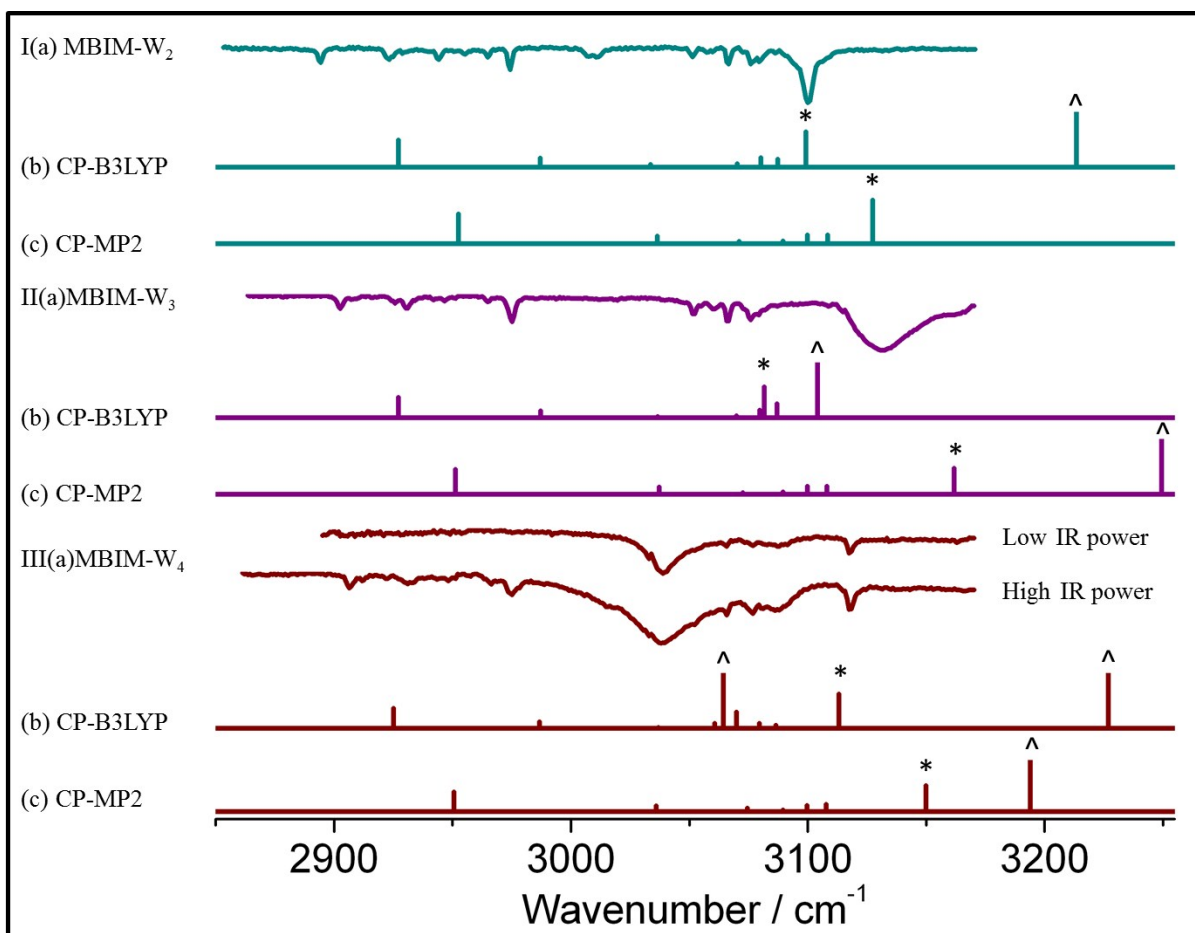


Figure S5.3: Observed FDIR spectra (Ia, IIa, IIIa) of MBIM- W_n ($n=2-4$) in the CH stretching region compared with the stick spectra computed at the cp-B3LYP/aug-cc-pVDZ (scaled by 0.9634) (Ib, IIb, IIIb) and cp-MP2/aug-cc-pVDZ (scaled by 0.9620) (Ic, IIc, IIIc) levels. Peaks marked ^ indicate a bonded O-H stretch whereas those marked * indicate an enhanced C(2)-H stretch. Trace III(a) gives the CH stretching region of the MBIM- W_4 cluster at low (< 1 mJ) and high IR power (~ 2 mJ), showing clearly the enhanced C(2)-H and the phenyl ring C-H modes at the base (high-energy side) of the hydrogen-bonded OH. The methyl stretches could also be seen at higher IR power.

For all the BIM- W_n and MBIM- W_n ($n=2-4$) complexes, structures of a homodromic W_n unit interacting with the parent molecule were also optimized. Structures involving linear water chains without any secondary stabilization, or water bridges deriving stabilization from a ring C-H or the π electron cloud were also considered. However, none of the structures agreed well with the vibrational spectra that were experimentally observed. Also, most of them were much higher up on the energy landscape compared to the global minimum structures to which the water clusters were assigned. In this section various possible structures for each cluster are presented along with the arguments either in their favor or against them.

Figures S6 to S11 show the other minimum energy structures of the BIM- W_{2-4} and MBIM- W_{2-4} clusters (along with the global minimum structure) and their calculated IR stick spectra at the B3LYP/aug-cc-pVDZ level. The binding energies of all the structures computed at the same level as well as using ω B97X-D and LC- ω PBE are provided in a table at the top of each figure. The optimized structures have been arranged in decreasing order of their binding energy (at B3LYP/aug-cc-pVDZ level) from 'T1' to 'Tn' ($n=7$ to 11 for various complexes) in each of the figures. Figures S6 to S11 also show the comparison of the computed stick spectra with the experimentally observed spectrum. The simulated spectra have also been arranged in decreasing order of the binding energy of the conformers. Thus, the topmost black trace in all the calculated spectra corresponds to the global minimum structure, T1 (with the exception of the BIM- W_3 complex for which T2 was predicted to be the global minimum at the said level of calculation). The stick IR spectra in gray correspond to other minimum energy structures which were not observed experimentally. The intensities of the computed frequencies in the stick spectra are provided on the logarithmic scale in order to make all the features prominent. A blue vertical bar has been used to denote the position of the N-H stretch in BIM monomer. The C(2)-H stretch of interest has been marked with a blue circle in the computed spectra. In cases where the most red-shifted bound OH encroaches into the CH region, a red circle has been used to highlight them so that they can be differentiated from the CH stretches. A discussion on the specific spectroscopic signatures or binding energy considerations that were used to overrule all optimized structures other than the global minima to which the clusters were assigned is provided after Figure S11.

The other minimum energy structures (T1 through T11) for all the complexes were also optimized at other levels of theory. The ZPE and BSSE-corrected binding energies (in kcal mol⁻¹) of these complexes are provided in Tables S2 to S7. In these tables, I and II denote the 6-311++G** and aug-cc-pVDZ basis sets, respectively.

BIM-W ₂ Binding energy (kcal mol ⁻¹)							
Level/ basis set	T1	T2	T3	T4	T5	T6	T7
B3LYP / II	11.27	9.83	9.09	8.87	5.58	4.84	4.57
ωB97X-D / II	13.59	12.14	11.01	12.35	7.33	T2	T4
LC-ωPBE / II	11.43	9.83	9.19	9.27	5.72	5.23	T4

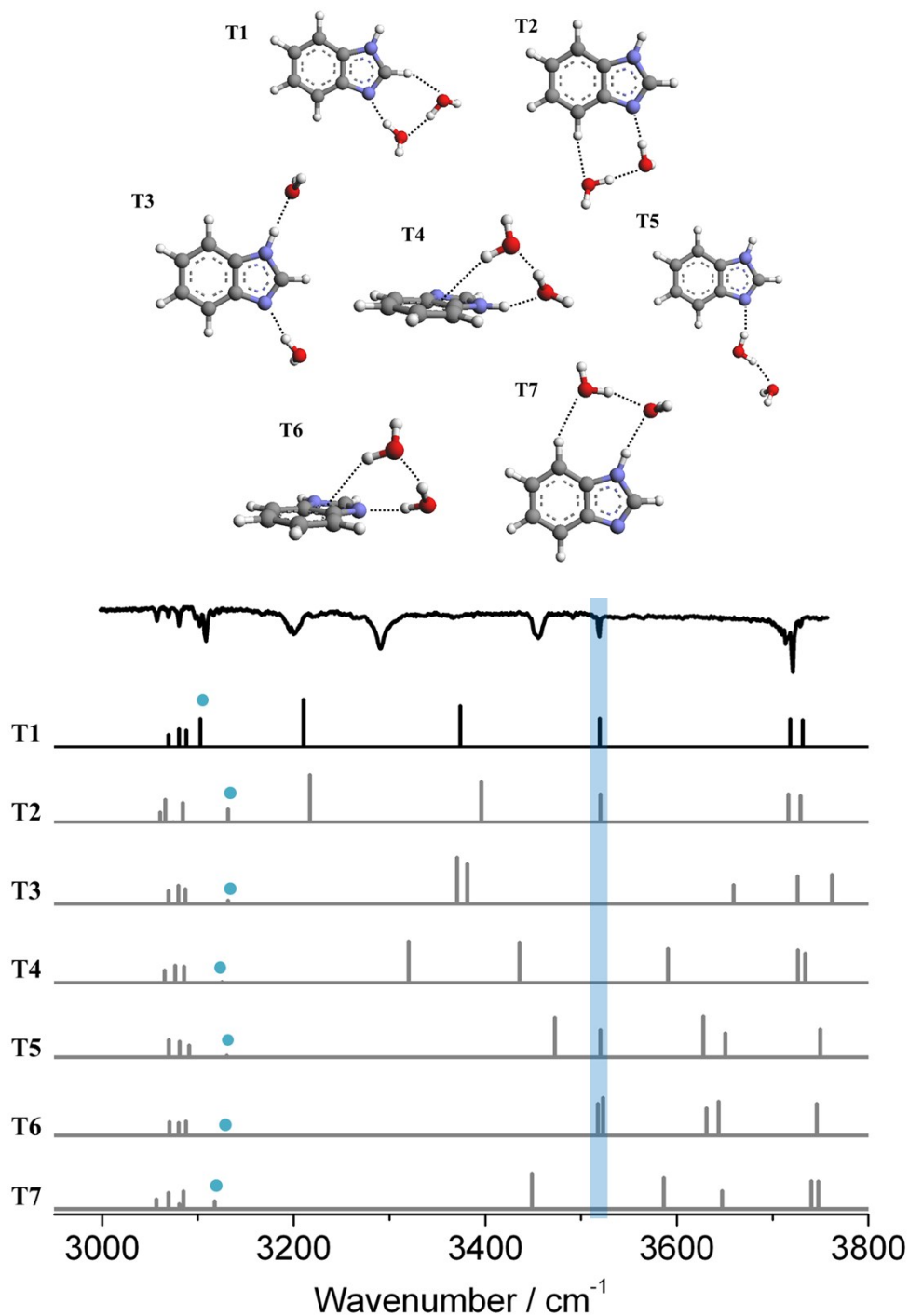


Figure S6 (Top) Optimized structures of BIM-W₂ computed at the B3LYP/ aug-cc-pVDZ level and (bottom) comparison of their computed IR spectra with the experimentally observed IR spectrum. The structures have been arranged in decreasing order of their binding energy from T1 to T7. The positions of the C(2)-H stretching frequencies are indicated by blue dots.

MBIM-W ₂ Binding energy (kcal mol ⁻¹)							
Level/ basis set	T1	T2	T3	T4	T5	T6	T7
B3LYP / II	11.57	10.06	6.37	6.08	5.75	5.09	4.20
ωB97X-D / II	13.75	12.20	10.29	9.16	7.34	T2	–
LC-ωPBE / II	11.73	10.07	7.31	6.56	5.94	5.42	4.56

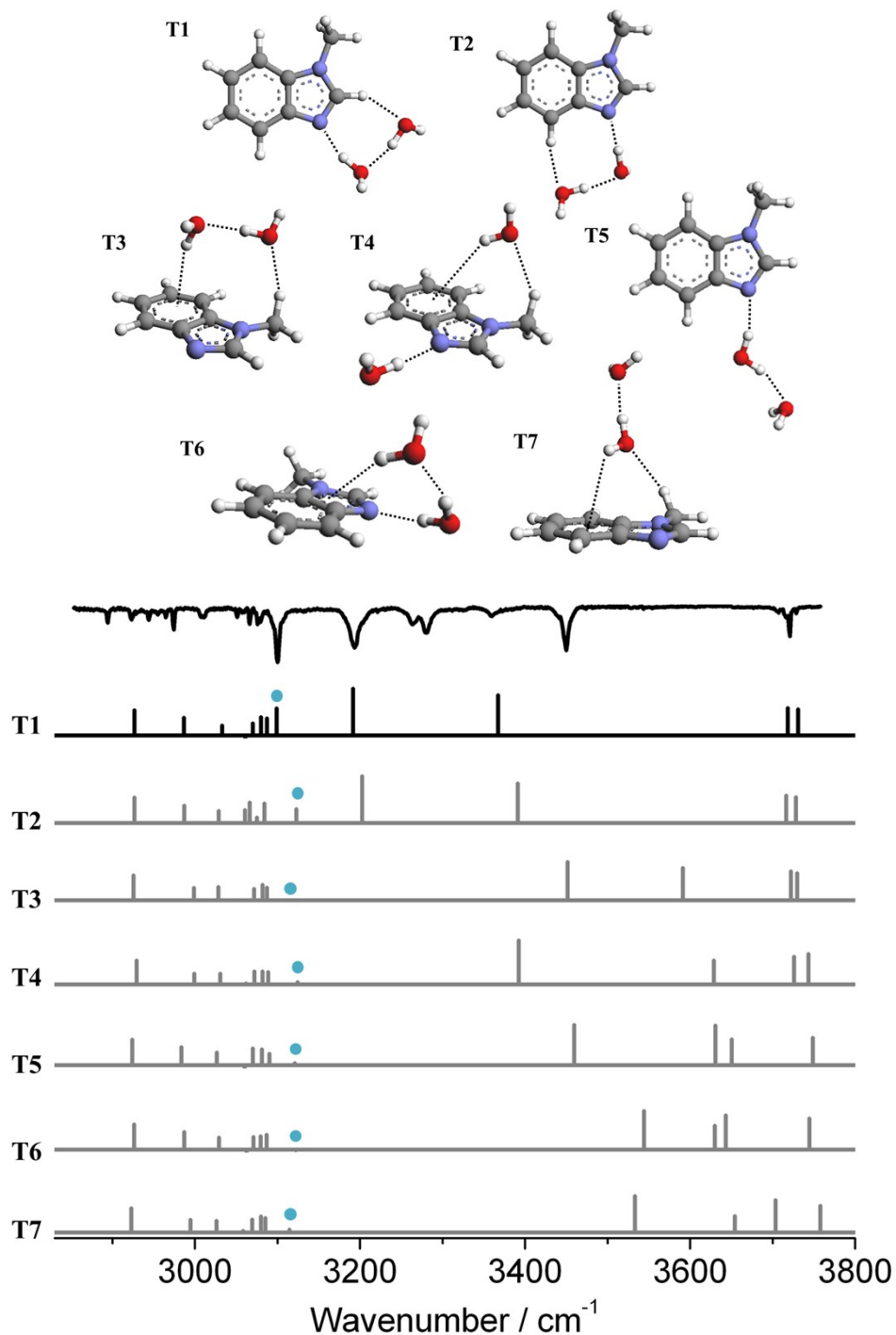


Figure S7 (Top) Optimized structures of MBIM-W₂ computed at the B3LYP/ aug-cc-pVDZ level and (bottom) comparison of their computed IR spectra with the experimentally observed IR spectrum. The structures have been arranged in decreasing order of their binding energy from T1 to T7. Blue dots indicate the position of the C(2)-H stretch in the various conformers.

BIM-W ₃ Binding energy (kcal mol ⁻¹)											
Level/ basis set	T1	T2	T3	T4	T5	T6	T7	T8	T9	T10	T11
B3LYP / II	17.46	18.10	15.66	15.61	14.73	14.42	14.29	14.23	13.86	13.61	9.50
ω B97X-D / II	21.73	21.09	18.91	T1	18.29	17.61	18.05	T2	T10	18.28	14.08
LC- ω PBE / II	18.08	18.15	15.95	16.42	15.03	14.52	14.48	T2	13.98	14.03	10.02

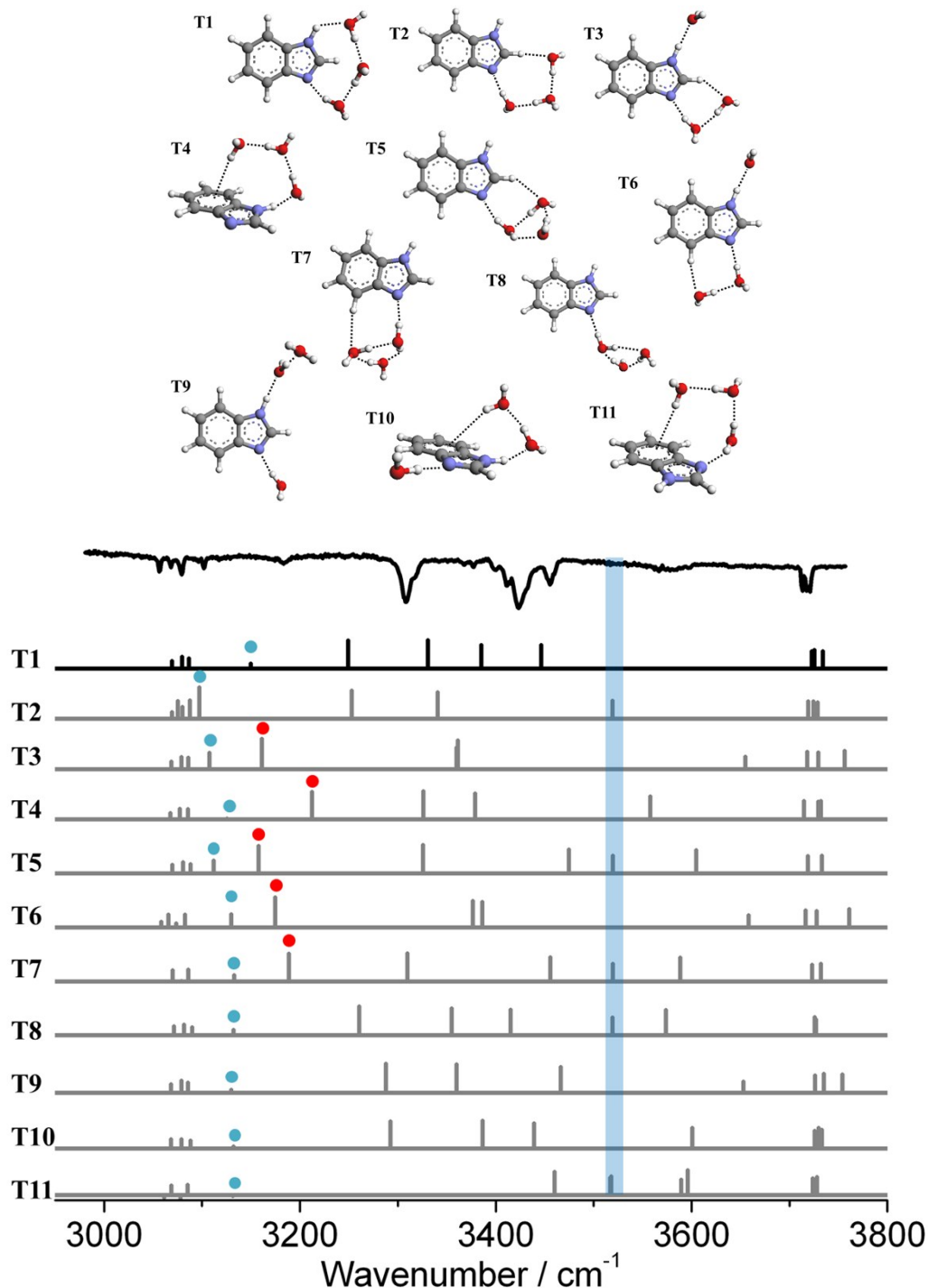


Figure S8 (Top) Optimized structures of BIM-W₃ computed at the B3LYP/ aug-cc-pVDZ level and (bottom) comparison of their computed IR spectra with the experimentally observed IR spectrum. The structures have been arranged in decreasing order of their binding energy from T1 to T11. Blue dots indicate the position of the C(2)-H stretch whereas red dots denote red-shifted bound OH stretches which encroach into the CH region of the spectrum.

MBIM-W ₃ Binding energy (kcal mol ⁻¹)											
Level/ basis set	T1	T2	T3	T4	T5	T6	T7	T8	T9	T10	T11
B3LYP / II	18.50	15.03	15.02	14.54	13.05	12.90	11.69	10.25	9.57	9.25	7.29
ω B97X-D / II	21.62	17.82	18.28	17.75	T3	17.06	15.77	13.70	14.59	12.35	T7
LC- ω PBE / II	18.62	14.94	15.29	14.71	T1	13.44	12.13	10.63	10.10	9.57	7.89

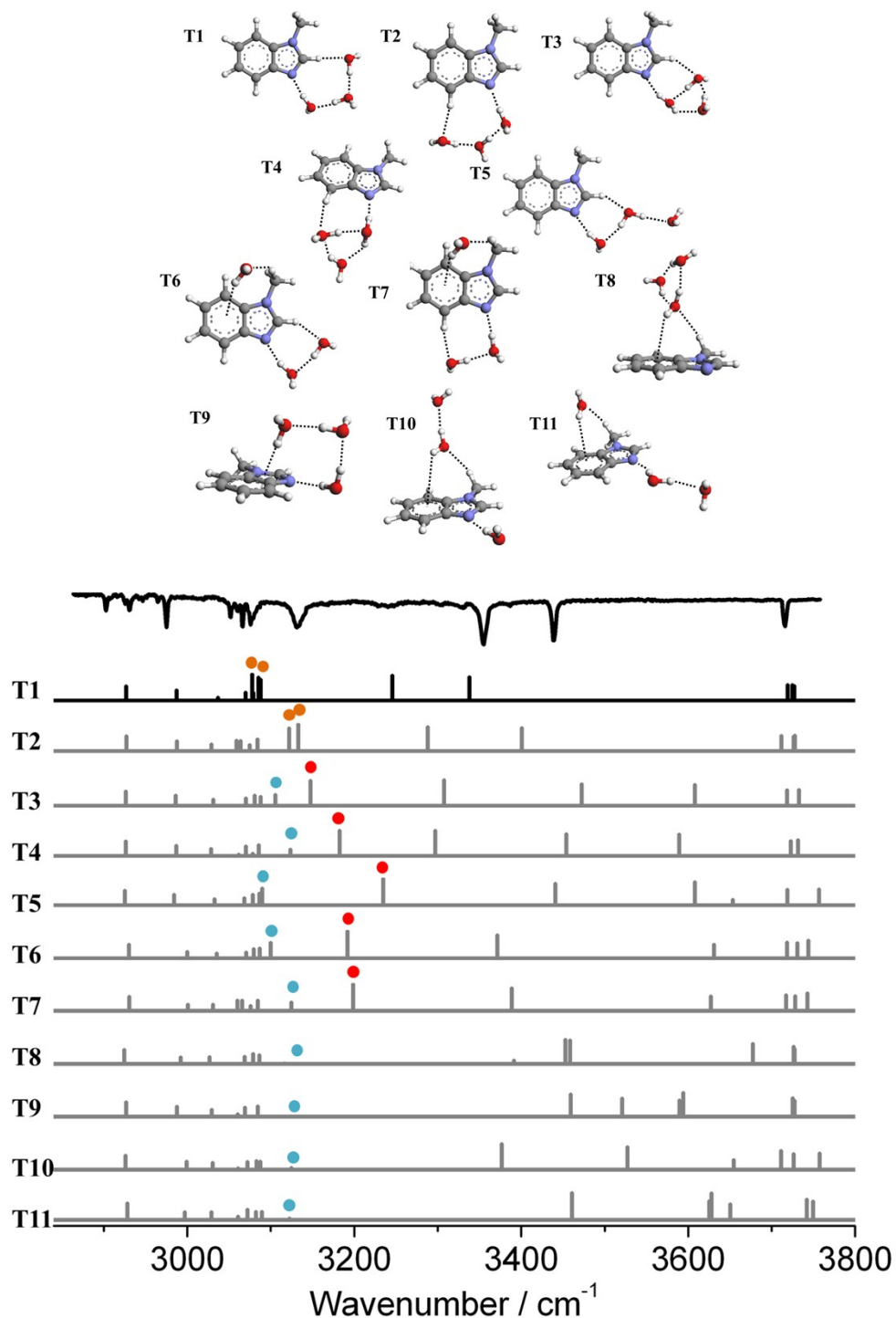


Figure S9 (Top) Optimized structures of MBIM-W₃ computed at the B3LYP/ aug-cc-pVDZ level and (bottom) comparison of their computed IR spectra with the experimentally observed IR spectrum. The structures have been arranged in decreasing order of their binding energy from T1 to T11. Blue dots denote the C(2)-H stretches, red dots denote red-shifted bound OH stretches which encroach into the CH region, and orange dots denote coupled bound-OH and CH stretches.

BIM-W ₄ Binding energy (kcal mol ⁻¹)										
Level/ basis set	T1	T2	T3	T4	T5	T6	T7	T8	T9	T10
B3LYP / II	26.27	22.88	22.82	21.73	21.72	21.27	21.20	19.28	19.07	18.84
ω B97X-D / II	31.21	T4	–	26.23	26.98	27.83	28.82	24.03	24.59	22.95
LC- ω PBE / II	26.64	T4	22.70	21.89	21.78	22.20	22.36	19.60	19.36	19.12

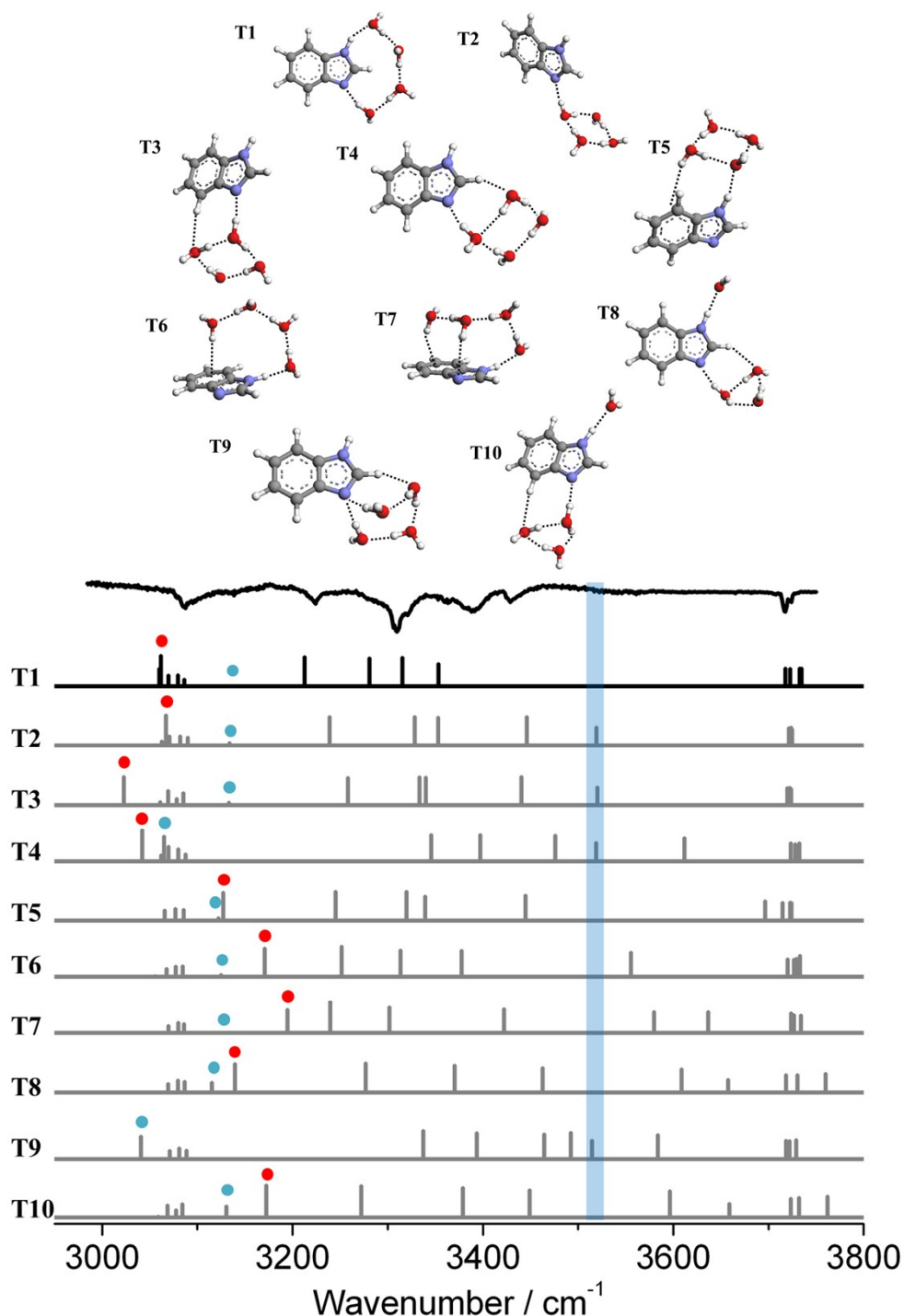


Figure S10 (Top) Optimized structures of BIM-W₄ computed at the B3LYP/ aug-cc-pVDZ level and (bottom) comparison of their computed IR spectra with the experimentally observed IR spectrum. The structures have been arranged in decreasing order of their binding energy from T1 to T10. Blue dots indicate the position of the C(2)-H stretch whereas red dots denote red-shifted bound OH stretches which encroach into the CH region.

MBIM-W ₄ Binding energy (kcal mol ⁻¹)											
Level/ basis set	T1	T2	T3	T4	T5	T6	T7	T8	T9	T10	T11
B3LYP / II	24.34	23.15	23.08	22.85	22.65	21.70	20.69	17.76	17.71	17.65	17.48
ω B97X-D / II	28.20	26.27	–	27.58	T8	T8	T8	23.96	26.12	25.18	–
LC- ω PBE / II	24.48	22.96	22.93	22.80	23.04	21.82	20.92	17.66	18.66	20.00	17.81

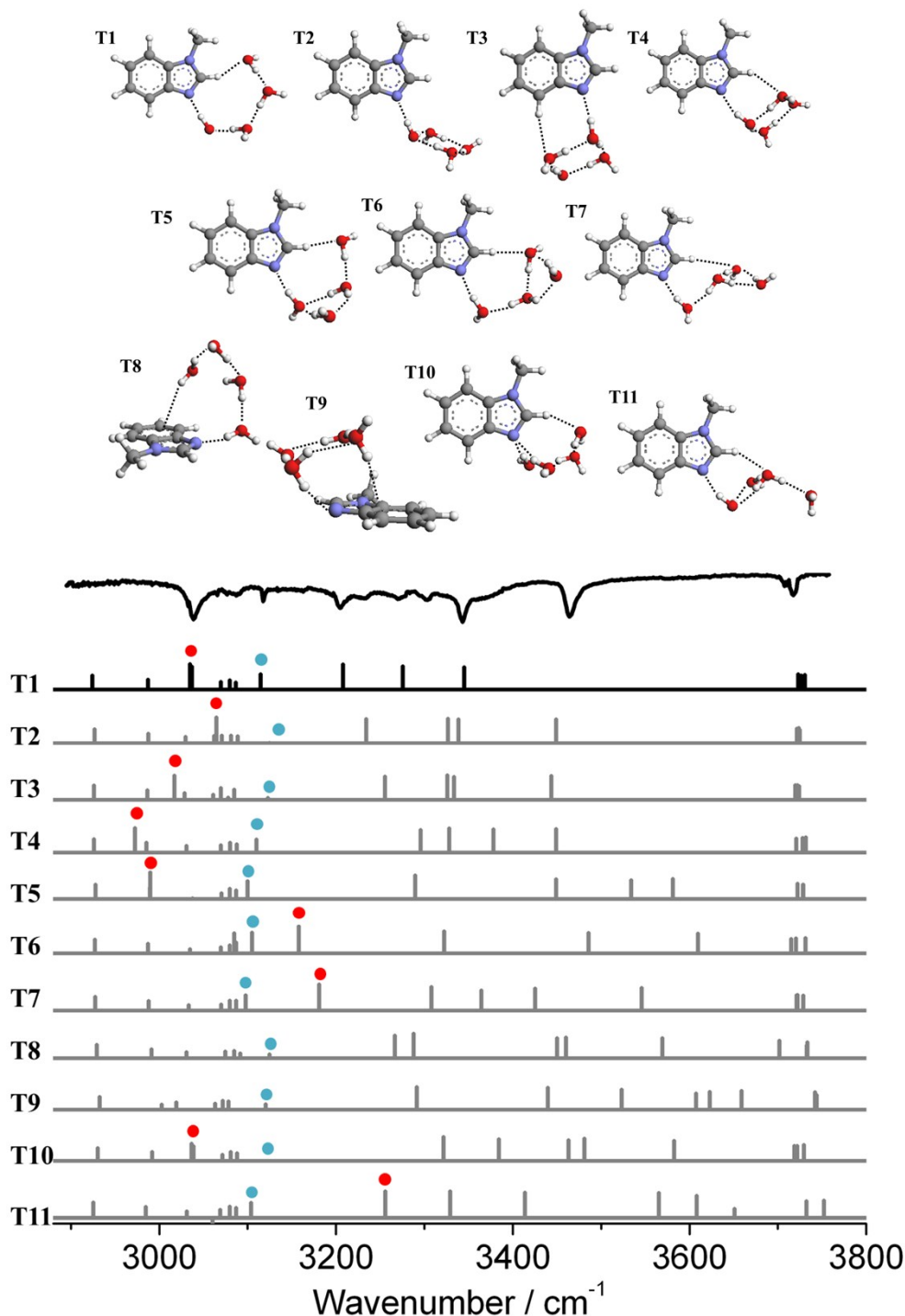


Figure S11 (Top) Optimized structures of MBIM-W₄ computed at the B3LYP/ aug-cc-pVDZ level and (bottom) comparison of their computed IR spectra with the experimentally observed IR spectrum. The structures have been arranged in decreasing order of their binding energy from T1 to T11. Blue dots indicate the position of the C(2)-H stretch whereas red dots denote red-shifted bound OH stretches which encroach into the CH region.

BIM-W₂

Structures T3, T4, and T7 cannot be possible structures for the BIM-W₂ complex as all of them contain an H-bonded N-H stretch whereas the NH stretch was found to be free in the observed IR spectrum. Structures T5 and T6 both show the presence of a free NH stretch; however, T5 predicts a bound OH···O stretch at 3627 cm⁻¹ and an O-H···N stretch at 3472 cm⁻¹ which were lower than the observed frequencies by 170 cm⁻¹ to 180 cm⁻¹. Similarly, T6 predicts all the bound O-H stretches (O-H···N, O-H···O and O-H···π) to appear at higher frequencies than that of the free NH, which is clearly not observed. Additionally, neither T5 nor T6 show any increased IR absorption in the CH region, which was a prominent feature in the IR spectra of the BIM-W₂ complex.

T2 had a very similar spectrum in the NH and OH regions to that of the global minimum structure T1 to which this complex was assigned. However, since the C(2)-H bond is not involved in H-bond formation in this particular structure, it does not predict much enhancement of the C(2)-H stretch whereas in the experiment, the intensity of the C(2)-H stretch well exceeded that of the ring C-H modes. Moreover, T2 turns out to be lower in energy than T1 by about 1.5 to 2 kcal mol⁻¹ at all levels of calculation (Table S2). Therefore, the global minimum structure T1 was assigned to this complex.

MBIM-W₂

Structures T3 to T7 were ruled out because they predicted the bound OH stretch to lie above 3400 cm⁻¹ and showed no enhancement in the intensity of the C(2)-H mode, whereas much higher red-shifts were observed in the O-H stretches in the experiment. The computed vibrational spectrum of the structure T2 was similar to that of T1 except for the lower intensity of the C(2)-H stretch based on which this structure was ruled out (coupled with the binding energy consideration which was lower for T2 compared to T1 by almost 1.5 to 2 kcal mol⁻¹).

It must be mentioned that the structure T2 for both BIM-W₂ and MBIM-W₂ produced a slight enhancement of the C(2)-H stretch, even though it is not involved in H-bonding in this particular structure. The enhancement is easy to perceive if the computed spectrum of T2 is compared with those of T3 to T7. This is because the C(2)-H derives some oscillator strength from the red-shifted bound O-H···N stretch in its proximity via a Fermi resonance.

BIM-W₃

Structures T2, T5, T7, T8, and T11 were ruled out as possible contenders for the BIM-W₃ complex as they all possess an unshifted NH stretch which was seen to be absent in the observed spectrum. T3, T6, and T9 were ruled out as they gave transitions corresponding to the free ν₁ and ν₃ modes of a water molecule which were not observed in the experiment. T4 and T10 were rejected as possibilities because both predicted a bound OH stretch between 3550 cm⁻¹ and 3600 cm⁻¹ which was not experimentally observed. Furthermore it must be noted that T2, T3, T5, and T6 showed the presence of an enhanced C(2)-H stretch as marked by the blue dot in the computed stick spectra. The only structure that faithfully reproduced the observed frequencies turned out to be the global minimum structure T1. It must be mentioned that the agreement of the bound OH stretches with the experiment was not best at this level of theory since it predicts four distinct bound OH/NH stretches whereas in the experiment one of the bound OH modes was obtained as a shoulder at 3411 cm⁻¹. More refined anharmonic calculations might be required to reproduce the positions of the coupled bound-OH/ NH stretches. The agreement between experiment and theory was found to be better at the cp-MP2/ aug-cc-pVDZ level as evident from Figure S4.2.

MBIM-W₃

Structures T3, T4, T5, T6, T7, T9, T10, and T11 were ruled out for this particular complex as they all showed the presence of one or more bonded OH stretches around $\sim 3600\text{ cm}^{-1}$, which was not seen in the experiment. T8 was eliminated as it showed the weak O-H \cdots O and O-H \cdots π bonded stretches to all appear above 3400 cm^{-1} , whereas the bound OH stretches registered higher red-shifts in the experiment.

Both T1 and T2 predicted the strongest O-H \cdots N H-bond to be mixed with the C(2)-H mode (the orange dots used to mark these features are an indication of mixed modes). While the C(2)-H is actually involved in H-bond formation in T1, it is free in T2 and gains intensity due to a Fermi resonance with the bound OH stretch. At other levels of calculation such as MP2 (not shown), the C(2)-H intensity was not seen to be affected in T2. Though the computed spectra of the T1 and T2 structures at B3LYP/ aug-cc-pVDZ are similar in the region of the bound OH, the latter was ruled out on the following two considerations,

- (a) T2 gave well-separated stretches in the free OH region (separated by 12 cm^{-1}) whereas in the experiment the free OH stretches appeared too close to be resolved in scans of step size 0.4 cm^{-1} .
- (b) The binding energy of T2 was computed to be 4 kcal mol^{-1} lower than that of T1. Such high energy conformers are not likely to compete with the global minimum structure in the cold temperature of the supersonic jet.

BIM-W₄

T2, T3, T4, and T9 were rejected as possible structural candidates of this complex because they showed the presence of a free NH stretch which was not present in the experimentally observed IR spectrum. T6, T7, T8, and T10 were ruled out because they showed one or more bound OH frequencies above the blue vertical bar marking the position of the free NH in the monomer, which was obviously not seen in the measured spectrum. Moreover, T8 and T10 contained one water molecule that acted as an acceptor alone. The only other structure T5 was ruled out because (a) it predicted much wider separation between the free OH stretches than experimentally observed, (b) it predicted the most red-shifted OH stretch to appear just above the aromatic CH stretches whereas experimentally the most red-shifted OH stretch encroached well into the CH region which is more accurately reflected by the global minimum structure T1, and (c) its binding energy was lower by $\sim 5\text{ kcal mol}^{-1}$ compared to the global minimum structure T1 which is a tall order for the typical temperatures in the molecular beam.

MBIM-W₄

Structures T5 through T11 were ruled out as they predicted one or more bound O-H stretches above 3500 cm^{-1} whereas the first bound OH appears in the spectrum at 3464 cm^{-1} . T2, T3, and T4 were rejected as possibilities because they predicted five bound OH stretches whereas only four were observed in the experiment. In addition, T2 and T3 did not predict any enhancement in the C(2)-H oscillator strength as it was not involved in H-bonding, which is contrary to the experimental signature of enhanced intensity in C(2)-H stretch. Even though T4 predicted an enhanced C(2)-H stretch, it was not accepted because (a) it showed five bound OH stretches, (b) the lowest frequency O-H \cdots N stretch was far too shifted to the red compared to the experiment and (c) its binding energy was ~ 3.5 to 4 kcal mol^{-1} lower than that of T1.

Figure S12 shows the computed normal mode eigenvectors (cp-MP2/ aug-cc-pVDZ) of the BIM- W_n and MBIM- W_n complexes ($n=2-4$). The water molecules are numbered 1, 2... from the N end to the N-H/ C(2)-H end.

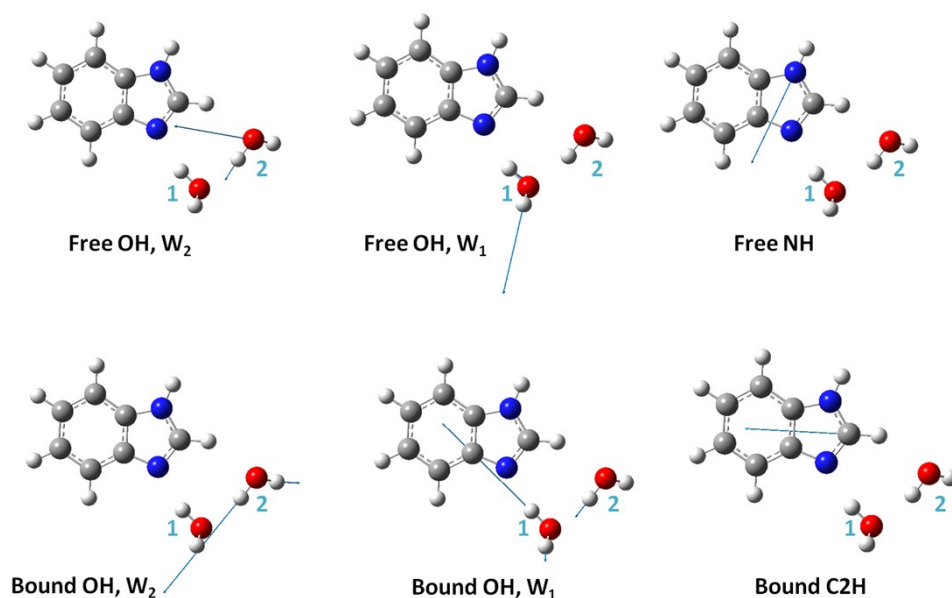


Figure S12.1. Normal mode eigenvectors of BIM- W_2 complex arranged in decreasing order of frequency.

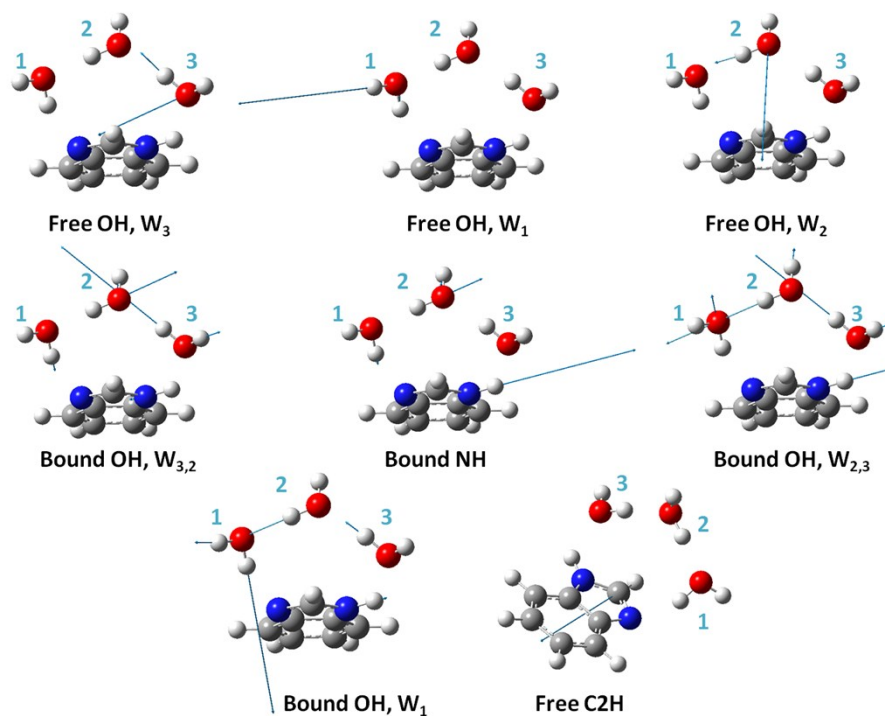


Figure S12.2. Normal mode eigenvectors of BIM- W_3 complex arranged in decreasing order of frequency.

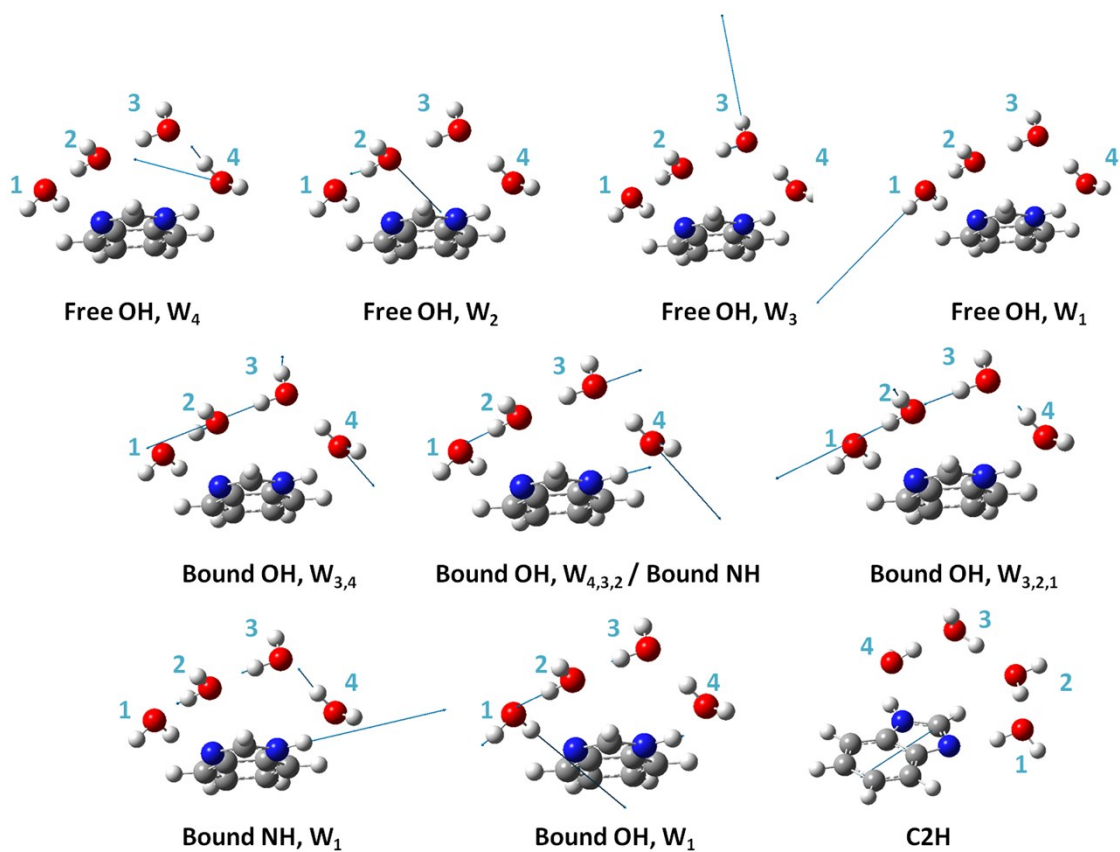


Figure S12.3. Normal mode eigenvectors of BIM- W_4 complex arranged in decreasing order of frequency.

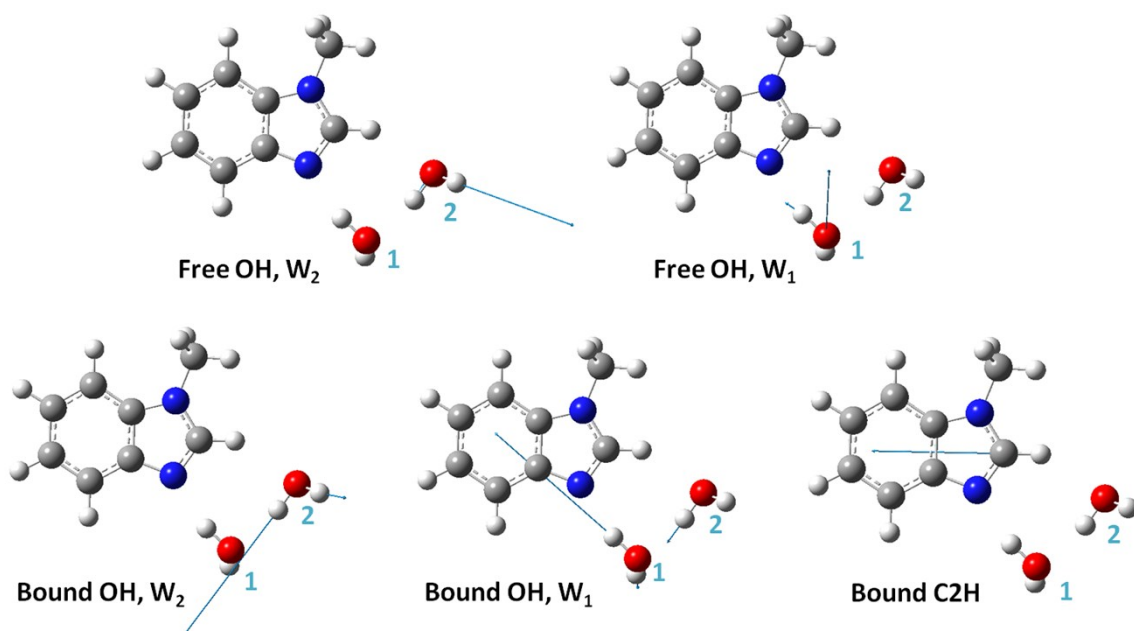


Figure S12.4. Normal mode eigenvectors of MBIM- W_2 complex arranged in decreasing order of frequency.

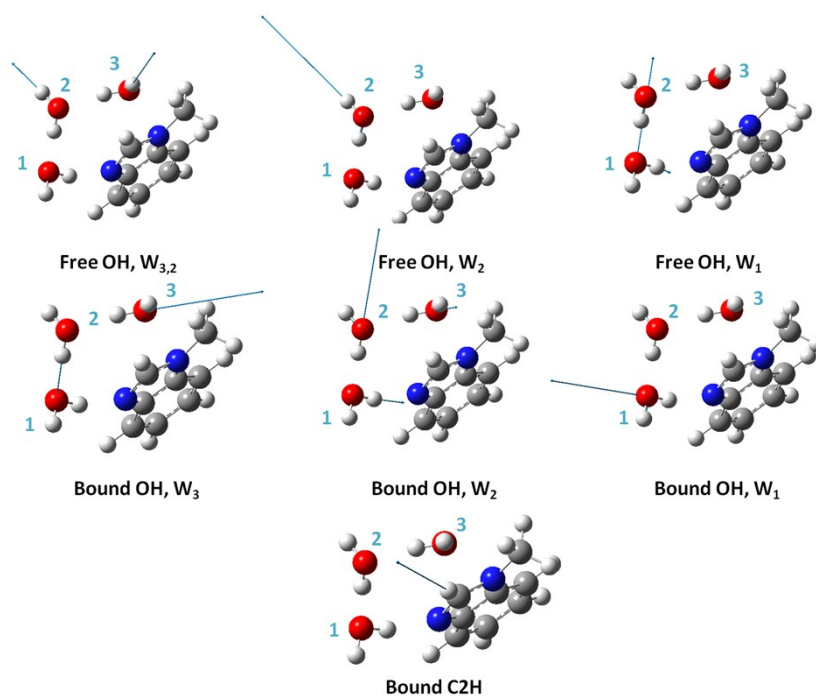


Figure S12.5. Normal mode eigenvectors of MBIM- W_3 complex arranged in decreasing order of frequency.

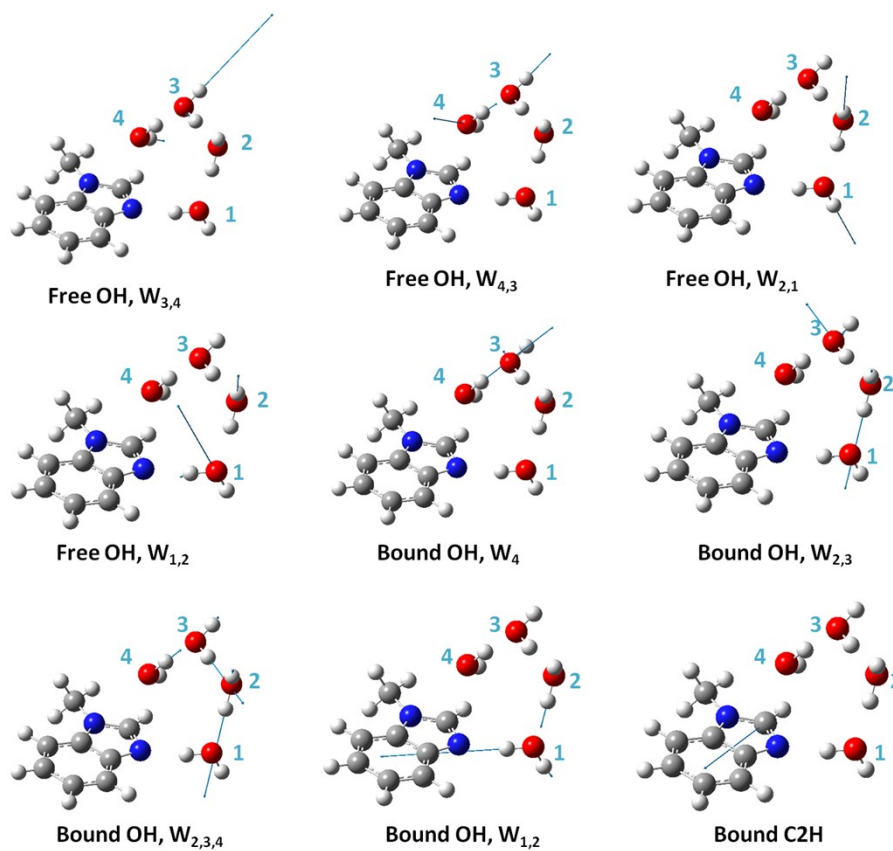


Figure S12.6. Normal mode eigenvectors of MBIM- W_4 complex arranged in decreasing order of frequency.

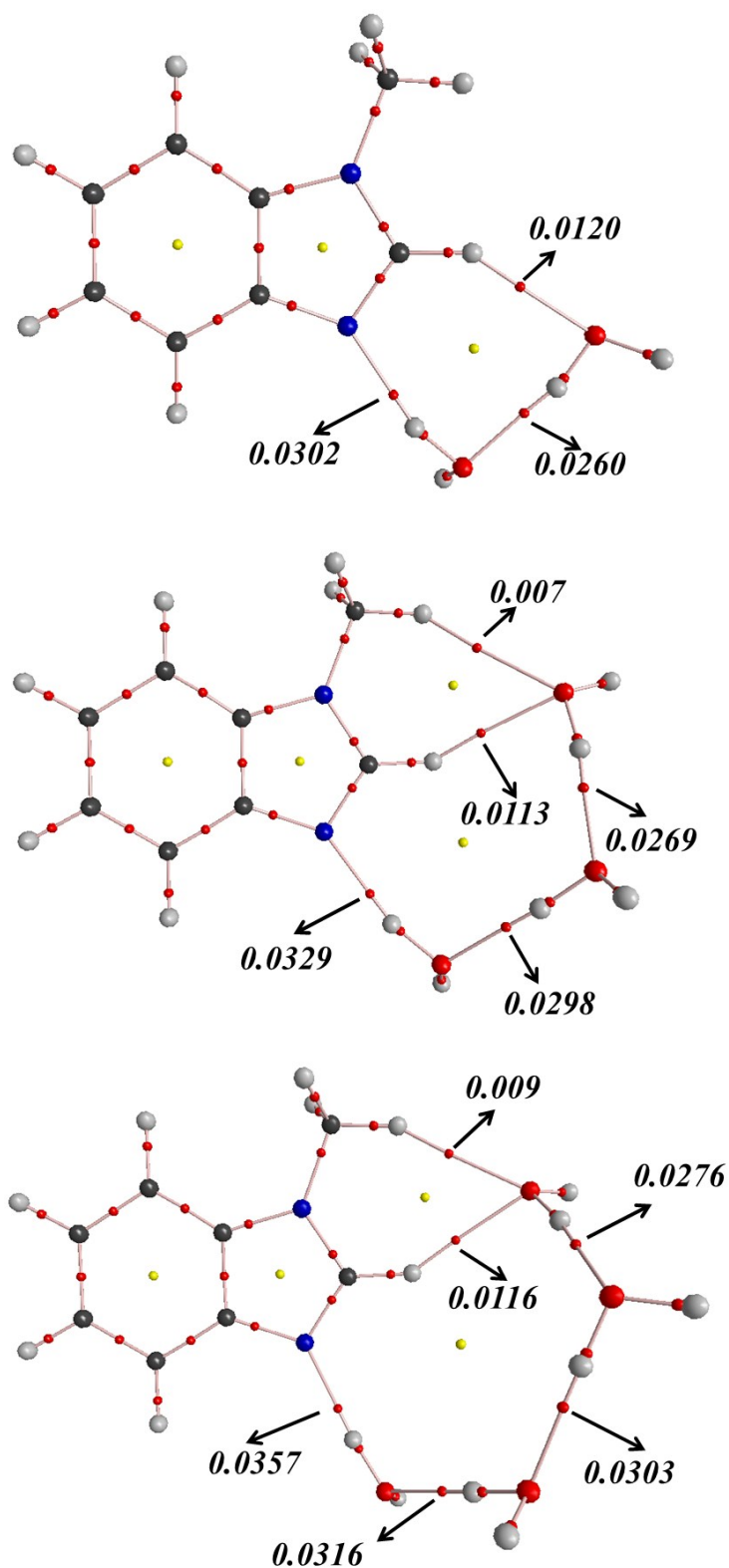


Figure S13: Molecular graphs of MBIM-W_n (n=2-4) obtained from QTAIM (Quantum theory of Atoms in Molecules) analysis using wavefunctions furnished at the cp-MP2/aug-cc-pVDZ level of theory. The (3,-1) bond critical points are denoted by red circles along the bond paths and the (3,+1) ring critical points are denoted by yellow circles. The values of the charge densities at the bond critical points are specified in italics. Secondary C-H(methyl)···O H-bonding interactions are identified in MBIM-W_{3,4}.

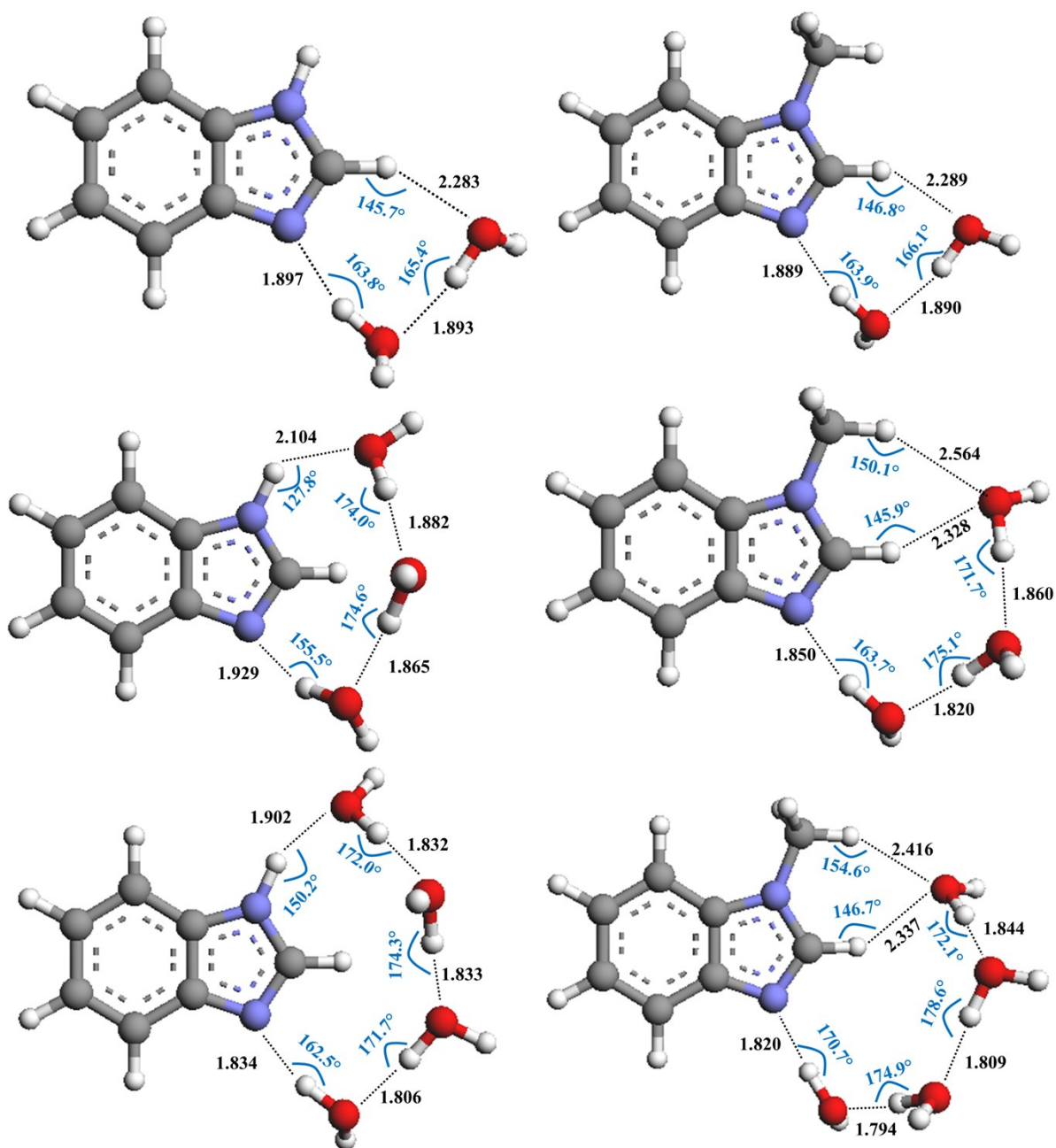


Figure S14: H-bond lengths and bond angles of the experimentally observed structures computed at the cp-MP2/aug-cc-pVDZ level of theory.

TABLES

Table S1: Assignments and positions of the transitions observed in the electronic spectra of BIM and MBIM water clusters

Peak Label	Assignment	Position (cm ⁻¹)	Peak Label	Assignment	Position (cm ⁻¹)
A'		35954	A		35712
A	BIM-W ₁	36126	B	MBIM-W ₁	35788
B		36171			
C	BIM-W ₂	36239	C	MBIM-W ₂	35881
D	BIM-W ₃	36196	D	MBIM-W ₃	35905
E	BIM-W ₄	36207	E	MBIM-W ₄	35893

Table S2 Binding energies (in kcal mol⁻¹) of various conformers of BIM-W₂ (shown in Figure S6) calculated at various levels. Some structures when optimized at certain levels were found to converge to other structures and have been indicated. Blanks in the table correspond to structures with imaginary frequencies or different from those considered in Figure S6.

Level/ basis set	T1	T2	T3	T4	T5	T6	T7
B3LYP / I	11.99	10.45	9.88	9.67	6.31	5.27	5.18
B3LYP / II	11.27	9.83	9.09	8.87	5.58	4.84	4.57
M06-2X / I	14.08	12.12	11.06	13.94	7.87	8.99	T4
M06-2X / II	12.92	10.93	9.64	12.28	T2	T2	–
ωB97X-D / I	14.39	12.69	11.94	13.35	8.00	T2	T4
ωB97X-D / II	13.59	12.14	11.01	12.35	7.33	T2	T4
LC-ωPBE / I	12.32	10.55	10.09	10.30	6.53	5.78	–
LC-ωPBE / II	11.43	9.83	9.19	9.27	5.72	5.23	T4
MP2 / I	10.62	9.18	9.46	10.68	5.82	T2	5.56
MP2 / II	11.68	10.21	10.01	11.07	6.45	–	T4

Table S3 Binding energies (in kcal mol⁻¹) of various conformers of MBIM-W₂ (shown in Figure S7) calculated at various levels. Some structures when optimized at certain levels were found to converge to other structures and have been indicated. Blanks in the table correspond to structures with imaginary frequencies or different from those considered in Figure S7.

Level/ basis set	T1	T2	T3	T4	T5	T6	T7
B3LYP / I	12.30	10.67	7.14	6.78	6.48	5.49	4.86
B3LYP / II	11.57	10.06	6.37	6.08	5.75	5.09	4.20
M06-2X / I	14.18	12.35	11.95	9.82	7.78	T2	7.19
M06-2X / II	13.20	11.11	10.77	8.68	T2	T2	6.16
ωB97X-D / I	14.58	12.87	11.63	9.84	7.88	T2	–
ωB97X-D / II	13.75	12.20	10.29	9.16	7.34	T2	–
LC-ωPBE / I	12.63	10.79	8.24	7.38	6.63	5.93	5.40
LC-ωPBE / II	11.73	10.07	7.31	6.56	5.94	5.42	4.56
MP2 / I	11.09	9.18	9.41	7.70	6.55	–	–
MP2 / II	11.98	10.50	9.61	8.50	6.59	–	–

Table S4 Binding energies (in kcal mol⁻¹) of various conformers of BIM-W₃ shown in Figure S8 calculated at various levels. Some structures when optimized at certain levels were found to converge to other structures and have been indicated. Blanks in the table correspond to structures with imaginary frequencies or different from those considered in Figure S8.

Level/ basis set	T1	T2	T3	T4	T5	T6	T7	T8	T9	T10	T11
B3LYP / I	18.81	19.14	16.69	16.70	25.78	15.39	15.41	15.41	15.12	14.94	10.48
B3LYP / II	17.46	18.10	15.66	15.61	14.73	14.42	14.29	14.23	13.86	13.61	9.50
M06-2X / I	24.09	21.62	19.45	23.08	19.86	17.93	19.19	18.33	16.74	19.89	15.32
M06-2X / II	21.96	T1	17.65	20.92	18.06	15.88	17.31	16.59	T1	17.63	14.03
ωB97X-D / I	23.12	22.22	19.98	T1	19.45	18.68	19.14	18.14	T10	19.53	14.99
ωB97X-D / II	21.73	21.09	18.91	T1	18.29	17.61	18.05	T2	T10	18.28	14.08
LC-ωPBE / I	19.72	19.40	17.17	T1	16.22	15.68	15.79	15.68	15.29	15.56	11.16
LC-ωPBE / II	18.08	18.15	15.95	16.42	15.03	14.52	14.48	T2	13.98	14.03	10.02
MP2 / I	18.20	16.24	15.29	17.14	13.95	14.30	13.78	13.14	10.09	15.37	10.13
MP2 / II	19.45	17.92	16.70	18.32	15.51	15.46	–	–	T10	16.03	11.48

Table S5 Binding energies (in kcal mol⁻¹) of various conformers of MBIM-W₃ shown in Figure S9 calculated at various levels. Some structures when optimized at certain levels were found to converge to other structures and have been indicated. Blanks in the table correspond to structures with imaginary frequencies or different from those considered in Figure S9.

Level/ basis set	T1	T2	T3	T4	T5	T6	T7	T8	T9	T10	T11
B3LYP / I	19.61	15.93	16.07	15.68	14.27	13.76	12.49	11.39	10.48	10.22	8.20
B3LYP / II	18.50	15.03	15.02	14.54	13.05	12.90	11.69	10.25	9.57	9.25	7.29
M06-2X / I	22.89	T4	19.78	19.14	16.71	18.16	16.39	18.85	16.01	T9	12.02
M06-2X / II	20.93	T4	18.12	17.28	14.91	16.70	15.17	17.28	14.83	T9	T7
ωB97X-D / I	23.10	18.71	19.64	19.00	16.97	17.75	16.71	15.14	15.33	13.68	–
ωB97X-D / II	21.62	17.82	18.28	17.75	T3	17.06	15.77	13.70	14.59	12.35	T7
LC-ωPBE / I	19.96	16.05	16.49	15.96	14.65	14.64	13.20	11.99	11.19	10.76	9.00
LC-ωPBE / II	18.62	14.94	15.29	14.71	T1	13.44	12.13	10.63	10.10	9.57	7.89
MP2 / I	17.46	13.56	14.34	13.87	12.71	13.85	13.11	–	10.80	T9	–
MP2 / II	18.88	T4	15.77	15.23	13.75	15.01	13.86	–	12.40	11.10	10.00

Table S6 Binding energies (in kcal mol⁻¹) of various conformers of BIM-W₄ shown in Figure S10 calculated at various levels. Some structures when optimized at certain levels were found to converge to other structures and have been indicated. Blanks in the table correspond to structures with imaginary frequencies or different from those considered in Figure S10.

Level/ basis set	T1	T2	T3	T4	T5	T6	T7	T8	T9	T10
B3LYP / I	28.43	24.31	24.16	23.50	23.17	22.78	22.52	20.62	20.25	20.35
B3LYP / II	26.27	22.88	22.82	21.73	21.72	21.27	21.20	19.28	19.07	18.84
M06-2X / I	33.22	T4	–	28.50	28.57	29.82	31.09	24.80	25.52	24.60
M06-2X / II	30.67	T4	–	25.12	26.20	27.54	28.87	22.69	23.54	22.13
ωB97X-D / I	33.27	T4	–	27.95	28.56	29.05	30.22	25.35	25.85	24.75
ωB97X-D / II	31.21	T4	–	26.23	26.98	27.83	28.82	24.03	24.59	22.95
LC-ωPBE / I	28.90	T4	24.20	24.38	23.50	T7	23.99	21.12	20.79	20.81
LC-ωPBE / II	26.64	T4	22.70	21.89	21.78	22.20	22.36	19.60	19.36	19.12
MP2 / I	25.42	T4	–	20.61	20.80	21.58	22.44	18.85	19.33	18.69
MP2 / II	27.26	T4	–	22.16	22.26	T7	24.80	20.54	20.76	20.20

Table S7 Binding energies (in kcal mol⁻¹) of various conformers of MBIM-W₄ shown in Figure S11 calculated at various levels. Some structures when optimized at certain levels were found to converge to other structures and have been indicated. Blanks in the table correspond to structures with imaginary frequencies or different from those considered in Figure S11.

Level/ basis set	T1	T2	T3	T4	T5	T6	T7	T8	T9	T10	T11
B3LYP / I	25.96	T4	24.42	24.60	24.44	23.07	22.37	19.61	19.04	20.83	18.86
B3LYP / II	24.34	23.15	23.08	22.85	22.65	21.70	20.69	17.76	17.71	17.65	17.48
M06-2X / I	29.48	27.47	28.11	T9	T8	T8	26.81	29.76	–	25.73	23.41
M06-2X / II	26.91	–	–	26.74	T8	T8	–	27.75	–	23.84	–
ωB97X-D / I	30.03	27.67	–	28.34	T8	T8	26.41	25.20	27.39	26.34	23.15
ωB97X-D / II	28.20	26.27	–	27.58	T8	T8	T8	23.96	26.12	25.18	–
LC-ωPBE / I	26.50	T4	24.44	24.36	25.22	23.51	22.81	T7	20.48	21.41	19.34
LC-ωPBE / II	24.48	22.96	22.93	22.80	23.04	21.82	20.92	17.66	18.66	20.00	17.81
MP2 / I	22.36	20.53	–	–	T8	T8	19.43	18.11	19.70	19.85	15.75
MP2 / II	24.38	22.31	–	–	T8	22.39	T8	20.44	22.60	21.42	18.48

Table S8: Experimentally observed and calculated frequencies (at cp-B3LYP/ aug-cc-pVDZ and cp-MP2/ aug-cc-pVDZ) of the free and bound OH, NH, and CH stretches in BIM- W_n and MBIM- W_n ($n=0,2-4$). The calculated frequencies were scaled by 0.9634 and 0.9620 at the B3LYP and MP2 levels, respectively, to match the calculated NH stretch in BIM with that observed (3519 cm^{-1}) experimentally. The same scaling factor was applied over the entire range of the spectrum. ('w' denotes weak, 'b' denotes broad)

BIM-W_n				
n	Observed	cp-B3LYP/ aug-cc-pVDZ (0.9634)	cp-MP2/ aug-cc-pVDZ (0.9620)	Assignment
0	3519 *3134* 3095 3080, 3068, 3055	3519 3124 3087, 3078, 3067, 3059 (w)	3519 3155 3110, 3101, 3090, 3081(w)	N-H *unassigned* C(2)-H C-H, phenyl
2	3721, 3713 3519 3455, 3290, *3200* 3109 3080, 3069, 3057	3729, 3719 3519 3386, 3230 3103 3088, 3080, 3069, 3062 (w)	3747, 3733 3518 3458, 3321 3138 3110, 3102, 3091, 3083 (w)	O-H, free N-H, free O-H, bound, *overtone, OH bend* C(2)-H, enhanced C-H, phenyl
3	3721, 3717, 3713 3455, 3423, 3411, 3308 - 3079, 3068, 3056	3732, 3724, 3721 3457, 3396, 3341, 3259 3152 3086, 3080, 3069, 3060 (w)	3746, 3738, 3735 3463, 3442, 3424, 3359 3171 3109, 3102, 3091, 3082 (w)	O-H, free N-H bound, O-H bound (mixed) C(2)-H C-H, phenyl
4	3724, 3722, 3718 (b) 3429, 3388, 3310, 3224, 3088 - -	3731, 3730, 3722, 3718 3369, 3327, 3285, 3238, 3091 3140 3086 (w), 3079, 3069, 3060 (w)	3746, 3739, 3737, 3729 3446, 3404, 3343, 3318, 3210 3161 3109, 3101, 3091, 3082 (w)	O-H, free N-H bound, O-H bound (mixed) C(2)-H C-H, phenyl
MBIM-W_n				
n	Observed	cp-B3LYP/ aug-cc-pVDZ (0.9634)	cp-MP2/ aug-cc-pVDZ (0.9620)	Assignment
0	*3132* 3103 3077, 3065, 3056 3047, 3004, 2968	3115 3087, 3079, 3068, 3059 (w) 3025, 2980, 2922	3141 3108, 3100, 3089, 3079 (w) 3066, 3032, 2950	*unassigned* C(2)-H C-H, phenyl C-H, methyl
2	3721, 3717 3450, *3281, 3264*, 3194 3100 3076, 3067, 3057 3051, 3011, 2974	3729, 3719 3380, 3213 3099 3087, 3080, 3070, 3061 (w) 3033, 2987, 2927	3746, 3732 3452, 3306 3128 3109, 3100, 3090, 3081 (w) 3071, 3037, 2953	O-H, free O-H, bound, *overtone, OH bend* C(2)-H, enhanced C-H, phenyl C-H, methyl
3	3716 (b) 3439, 3355, 3131 - 3076, 3067, 3061 3052, 2975	3726, 3723, 3718 3351, 3262, 3104 3081 3087, 3079, 3070, 3061 (w) 3036, 2987, 2927	3740, 3739, 3734 3448, 3383, 3250 3162 3108, 3100, 3090, 3081 (w) 3071, 3037, 2953	O-H, free O-H, bound C(2)-H, enhanced C-H, phenyl C-H, methyl
4	3717 (b), 3710, 3707 3464, 3343, 3205, 3039 3117 3077, 3066 2975	3728, 3725, 3722, 3720 3359, 3292, 3227, 3064 3113 3086, 3079, 3070, 3060 (w) 3037, 2986, 2925	3742, 3741, 3735, 3734 3441, 3395, 3345, 3194 3150 3108, 3100, 3090, 3081 (w) 3075, 3036, 2951	O-H, free O-H, bound C(2)-H, enhanced C-H, phenyl C-H, methyl

References

- [1] L. S. Rothman, I. E. Gordon, A. Barbe, D. C. Benner, P. E. Bernath, M. Birk, V. Boudon, L. R. Brown, A. Campargue, J. P. Champion, K. Chance, L. H. Coudert, V. Dana, V. M. Devi, S. Fally, J. M. Flaud, R. R. Gamache, A. Goldman, D. Jacquemart, I. Kleiner, N. Lacome, W. J. Lafferty, J. Y. Mandin, S. T. Massie, S. N. Mikhailenko, C. E. Miller, N. Moazzen-Ahmadi, O. V. Naumenko, A. V. Nikitin, J. Orphal, V. I. Perevalov, A. Perrin, A. Predoi-Cross, C. P. Rinsland, M. Rotger, M. Simeckova, M. A. H. Smith, K. Sung, S. A. Tashkun, J. Tennyson, R. A. Toth, A. C. Vandaele, J. Vander Auwera, *Journal of Quantitative Spectroscopy & Radiative Transfer* **2009**, *110*, 533.
- [2] M. J. Frisch, G. W. Trucks, H. B. Schlegel, G. E. Scuseria, M. A. Robb, J. R. Cheeseman, G. Scalmani, V. Barone, B. Mennucci, G. A. Petersson, H. Nakatsuji, M. Caricato, X. Li, H. P. Hratchian, A. F. Izmaylov, J. Bloino, G. Zheng, J. L. Sonnenberg, M. Hada, M. Ehara, K. Toyota, R. Fukuda, J. Hasegawa, M. Ishida, T. Nakajima, Y. Honda, O. Kitao, H. Nakai, T. Vreven, J. A. Montgomery Jr., J. E. Peralta, F. Ogliaro, M. Bearpark, J. J. Heyd, E. Brothers, K. N. Kudin, V. N. Staroverov, R. Kobayashi, J. Normand, K. Raghavachari, A. Rendell, J. C. Burant, S. S. Iyengar, J. Tomasi, M. Cossi, N. Rega, J. M. Millam, M. Klene, J. E. Knox, J. B. Cross, V. Bakken, C. Adamo, J. Jaramillo, R. Gomperts, R. E. Stratmann, O. Yazyev, A. J. Austin, R. Cammi, C. Pomelli, J. W. Ochterski, R. L. Martin, K. Morokuma, V. G. Zakrzewski, G. A. Voth, P. Salvador, J. J. Dannenberg, S. Dapprich, A. D. Daniels, O. Farkas, J. B. Foresman, J. V. Ortiz, J. Cioslowski and D. J. Fox, Gaussian 09, Revision C.01, 2009, Inc., Wallingford CT, 2010.
- [3] F. O. Talbot, J. P. Simons, *European Physical Journal D* **2002**, *20*, 389.